INL/EXT-21-63772-Revision-0

Development and Demonstration of a Reduced-Order PWR Power Dispatch Simulator

August 2021

Roger Lew, Bikash Poudel, Stephen Hancock, Yusheng Luo, Tyler L Westover

Changing the World's Energy Future

Idaho National Laboratory

INL is a U.S. Department of Energy National Laboratory operated by Battelle Energy Alliance, LLC

INL/EXT-21-63772-Revision-0

Development and Demonstration of a Reduced-Order PWR Power Dispatch Simulator

Roger Lew, Bikash Poudel, Stephen Hancock, Yusheng Luo, Tyler L Westover

August 2021

Idaho National Laboratory
Idaho Falls, Idaho 83415

http://www.inl.gov

Prepared for the
U.S. Department of Energy
Under DOE Idaho Operations Office
Contract DE-AC07-05ID14517

INL/EXT-21-63772
Revision 0

Light Water Reactor Sustainability Program

Development and Demonstration of a Reduced-Order PWR Power Dispatch Simulator

Reviewing Official: Sherman J. Remer
Date: 07/31/2021

July 2021

U.S. Department of Energy
Office of Nuclear Energy

PROJECT CONTROLLED INFORMATION

INL/EXT-21-63772
Revision 0

Development and Demonstration of a Reduced-Order PWR Power Dispatch Simulator

Roger Lew, Bikash Poudel, Tyler Westover, Stephen Hancock, Yusheng Luo

Prepared for the
U.S. Department of Energy
Office of Nuclear Energy

SUMMARY

This report describes the development, modeling, and results of a reduced-order thermal power dispatch pressurized water reactor (RO-TPD-PWR) power plant simulator that incorporates coupled electrical and thermal power dispatch to an industrial process. The simulator is built on models that have been developed in previous work, including a Rancor Microworld model previously developed by INL and the University of Idaho [1] and reactor core and secondary system models that have been published previously [2]. The simulator also includes a scalable model of a high temperature electrolysis (HTE) system that has been developed at INL. A particular benefit of the Rancor Microworld model is that it is compatible with a human-system interface (HMI) that has already been developed by the Human System Simulation Laboratory (HSSL) at INL that can emulate the control room of a PWR for realistic human-in-the-loop studies with mock nuclear power plant operating procedures. The results of these human-in-the-loop tests will be compared with similar tests using a commercial full-scope generic PWR (GPWR) simulator that has been modified to include thermal power dispatch, referred to as the TPD-GPWR [3, 4].

A key purpose of the RO-TPD-PWR simulator is that its relative simplicity allows it scale between lab-size equipment (~100 kW) and full-scale nuclear power plants (~1 GW) by adjusting only a few parameters in the models, such as fluid masses and heat exchanger areas. The RO-TPD-PWR simulator will be used to guide the controls of lab tests, so that equipment in those tests, such as the Thermal Energy Distribution System (TEDS) and pilot-scale high temperature electrolysis (HTE) units at scales of 50-250 kW, may operate in a manner that is relevant to full-scale PWR operations. By including operators, hardware and simulation in a single test, assumptions and idealized conditions in full-scope, high-fidelity PWR simulators can be tested using the RO-TPD-PWR simulator. For example, flow and pressure measurements in real pipes have uncertainty and fluctuations that may not be captured by computer simulations. Similarly, the behavior of real valves, actuators, and pumps can be different than that of idealized simulations. Physical tests with human operators and real valves, lines and heat exchangers assist understanding how to safely maintain the NPP at near 100% thermal power output while transitioning between TPD operating modes. To accomplish the goals described above, it is anticipated that the RO-TPD-PWR simulator must be able to match predictions of the full-scope TPD-GPWR simulator and also the lab-scale equipment within +/-15% (greater than 85% agreement for key parameters, such as the mass flow rates and fluid enthalpies in the main steam line, turbine system, and the thermal power dispatch system. As shown below, the RO-TPD-PWR simulator achieves these requirements.

Simulations were performed for 15% and 50% thermal power dispatch (*%TPD* = 15% and 50%, respectively). Figure ES-1 shows predicted steady-state values of mass flow in the main steam line and the turbine system for 0%, 15%, and 50% TPD. Prediction results are compared with those from the full-scope TPD GPWR simulator (labeled as “Hancock, et al.” [4]) and also with those of a previous analysis of a generic PWR (Ibrahim et al. for 0% TPD only). Results from two different versions of the RO-TPD-GPWR simulator are shown in Figure ES-1, labeled “RO, linear” and “RO, nonlinear.” The differences between the models is explained in Sections 3 and 4. All models show that mass flow in the main steam line decreases as flow in the thermal power dispatch (TPD) system increases because increasing flow in the TPD system removes steam from the turbine system that supports the feedwater heaters and causes the temperature of the feedwater entering the steam generator to decrease. Decreasing the feedwater temperature entering the steam generator causes a decrease of steam flow in the main steam line because the heat from the reactor is steady, so that heat provided by the steam generator to the main steam line is limited. The decrease in steam flow through the main steam line and turbine system with increasing steam flow in the XSL is evident in Figure ES-1. The nonlinear version of the RO-TPD-PWR simulator, which more accurately accounts for steam flow impacts in the feedwater heaters, shows better agreement to predictions of steam flow in the main steam line obtained from the full-scope TPD-GPWR simulator (Hancock, et al.) than does the linear version of the RO-TPD-PWR simulator that assumes the ratios of

flows in the feedwater heaters is fixed, regardless of flow in the TPD system (labelled "RO, linear" in Figure ES-1). In fact, for both 15% and 50% TPD, the error of the "RO, nonlinear" model for main steam flow is less than half that of the "RO, linear" model, compared to results from Hancock, et al. Interestingly, however, the predictions of steam flow in the turbine system from the "RO, nonlinear" model appear to be somewhat poorer than those of the "RO, linear" model. The differences, however, are moderate, and the discrepancies between all turbine steam flow predictions are less than 10% of the full turbine steam flow.

As expected, the power extracted from the turbine system decreases as steam flow to the turbine system decreases and steam flow to the TPS system increases. Figure ES-2 shows the predicted percent decrease in turbine power output for 15% and 50% TPD based on the full-scope TPD-GPWR simulator ("Hancock, et al.) and the two versions of the RO-TPD-PWR simulator. Predictions of turbine power output from the nonlinear version of the RO-TPD-PWR simulator most closely match those of the full-scope TPD-GPWR simulator, although discrepancies from both models are less than 7% of the full turbine power output. The ability of the model to match experimental measurements using pilot-scale equipment at INL will be established when that data becomes available. The Thermal Energy Distribution System (TEDS) is currently being commissioned and operational data is expected by September 2021. INL is also working with Bloom Energy to install a 100 kW high temperature electrolysis (HTE) unit at INL in August of 2021, and data from that system is also expected to also be available by September 2021 to demonstrate the ability of the RO-TPD-PWR simulator to match measurements of relevant pilot-scale equipment.

A final point is that the relative simplicity of the RO-TPD-PWR simulator has proven highly valuable in interpreting and explaining results obtained from the full-scope TPD-GPWR simulator. The RO-TPD-PWR simulator has proven beneficial in explaining nuanced key relationships between parameters, includes those between steam flows in the TPD system, turbine system, feedwater heaters and the main steam lines.

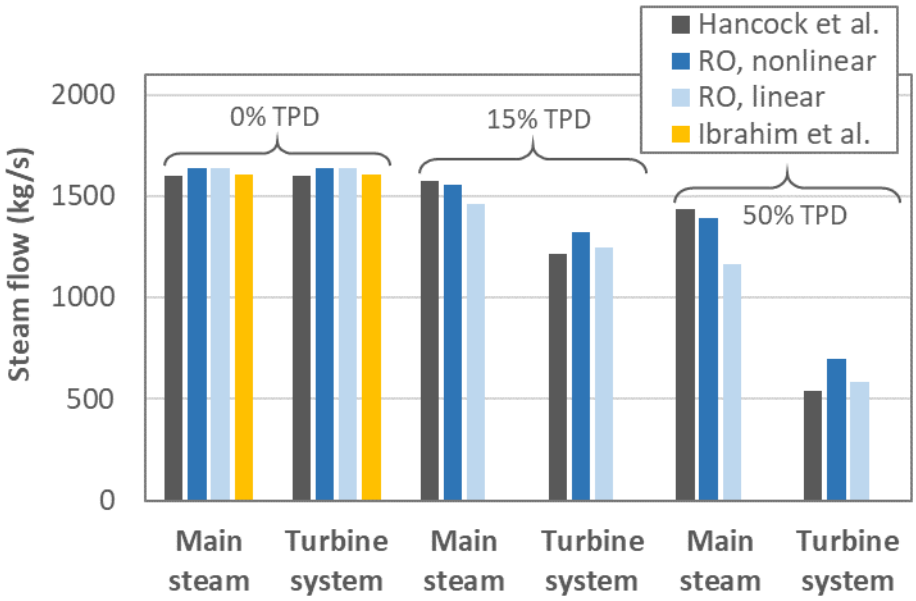

Figure ES-1. Predicted steam flow in the main steam line and turbine system for 0%, 15% and 50% TPD according to a full-scope TPD-GPWR simulator (Hancock et al), an approximate PWR mathematical model proposed by Ibrahim et al (0% TPD only) [5], and two versions of the RO-TPD-PWR simulator.

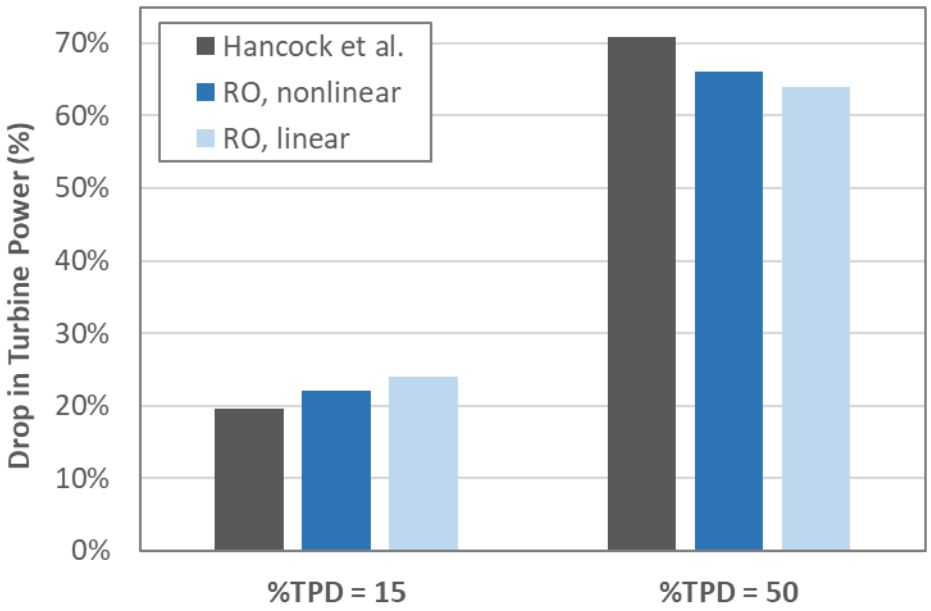

Figure ES-2. Predicted drop in turbine power output for 15% and 50% TPD according to a full-scope TPD-GPWR simulator (Hancock et al) and two versions of the RO-TPD-PWR simulator.

CONTENTS

FIGURES

TABLES

ACRONYMS

BOP	balance of plant
DI	deionized
DHL	delivery heat loop
DOE	Department of Energy
DRTS	digital real time simulator
DSL	delivery steam line
FDR HTR	feed water heater
HP	high pressure
HSI	human/system interface
HSSL	Human System Simulation Laboratory
HTSE	high-temperature steam electrolysis
INL	Idaho National Laboratory
LP	Low pressure
LWR	light-water reactor
MOV	motor operated valve
MSR	moisture separator reheater
MSH	min steam header
MSIV	main steam isolation valve
NPP	nuclear power plant
NPS	national pipe standard
PFD	process-flow diagram
PORV	pressure operated relief valve
PWR	pressurized water reactor
P&ID	piping and instrumentation diagram
TBV	turbine bypass valve
TCV	turbine control valve
TPD	thermal power dispatch
U.S.	United States (of America)
XSL	extraction steam line
tpd	Tonnes per day

Development and Demonstration of a Reduced-Order PWR Power Dispatch Simulator

1. INTRODUCTION

This report describes the development, modeling, and results of a reduced-order thermal power dispatch pressurized water reactor (RO-TPD-PWR) power plant simulator that incorporates coupled electrical and thermal power dispatch to an industrial process. The simulator is built on models that have been developed in previous work, including a Rancor Microworld model previously developed by INL and the University of Idaho [1] and reactor core and secondary system models that have been published previously [2]. The simulator also includes a scalable model of a high temperature electrolysis (HTE) system that has been developed at INL. A particular benefit of the Rancor Microworld model is that it is compatible with a human-system interface (HMI) that has already been developed by the Human System Simulation Laboratory (HSSL) at INL that can emulate the control room of a PWR for realistic human-in-the-loop studies with mock nuclear power plant operating procedures. The results of these human-in-the-loop tests will be compared with similar tests using a commercial full-scope generic PWR (GPWR) simulator that has been modified to include thermal power dispatch, referred to as the TPD-GPWR [3, 4]. The simplicity of the RO-TPD-PWR helps to better understand and verify the results of the TPD-GPWR, which employs >1,000 variables and has much greater complexity. A second key purpose of the RO-TPD-PWR simulator is that its relative simplicity allows it scale between lab-size equipment (~100 kW) and full-scale nuclear power plants (~1 GW) by adjusting only a few parameters in the models, such as fluid masses and heat exchanger areas. The RO-TPD-PWR simulator will be used to guide the controls of lab tests, so that equipment in those tests, such as the Thermal Energy Distribution System (TEDS) and pilot-scale high temperature electrolysis (HTE) units at scales of 50-250 kW, may operate in a manner that is relevant to full-scale PWR operations. To accomplish the goals described above, it is anticipated that the RO-TPD-PWR simulator must be able to match predictions of the full-scope TPD-GPWR simulator and also the lab-scale equipment within +/-15% (greater than 85% agreement for key parameters, such as the mass flow rates and fluid enthalpies in the main steam line, turbine system, and the thermal power dispatch system.

The design requirements for the RO-TPD-PWR are similar to those of the TPD-GPWR and have been presented in a previous report [3]. Namely, the requirements ensure multiple purposes are accomplished, including safety of the NPP and efficient use of nuclear energy for the industrial process. As described further below, the design requirements do not necessarily ensure that the NPP operates at maximum efficiency during thermal power dispatch operations (TPD). A leading requirement that drives the design is that the reactor power and the primary system of the PWR are maintained at or near the 100% steady power condition while the secondary system is maneuvered to allow for thermal and electrical power dispatch to the coupled industrial process.

The primary and secondary systems of the RO-TPD-PWR simulator are described in detail in the sections below. A simplified diagram of a representative system is shown in Figure 1-1. An extraction heat exchanger uses steam from the PWR to boil demineralized water for the HTE plant. The hot side fluid in the extraction heat exchanger comes from the main steam line of the NPP through an extraction steam line (XSL) and is sent to the condenser after it exits the extraction heat exchanger. The cold side fluid enters as demineralized water and exits as superheated steam that is sent to the HTE plant. In reality, three separate heat exchangers would be needed in practice for this operation. The first heat exchanger preheats the demineralized water, the second heat exchanger boils the demineralized water, and the third heat exchanger superheats the demineralized steam to send to the HTE plant. In this preliminary version of the RO-TPD-PWR, all three operations are simplified to a single thermal power extraction heat

exchanger. The three separate heat transfer functions may be separated in a future version of the RO-TPD-PWR, if it is determined beneficial to simulate the details of the heat exchangers.

A pressure station is placed at the hydrogen plant to regulate the pressure of the steam entering the hydrogen production process. The industrial heat user, in this case a high temperature steam electrolysis (HTSE) plant that produces hydrogen and oxygen from de-ionized or demineralized water, is not explicitly simulated in this report but is included as a transient heat sink.

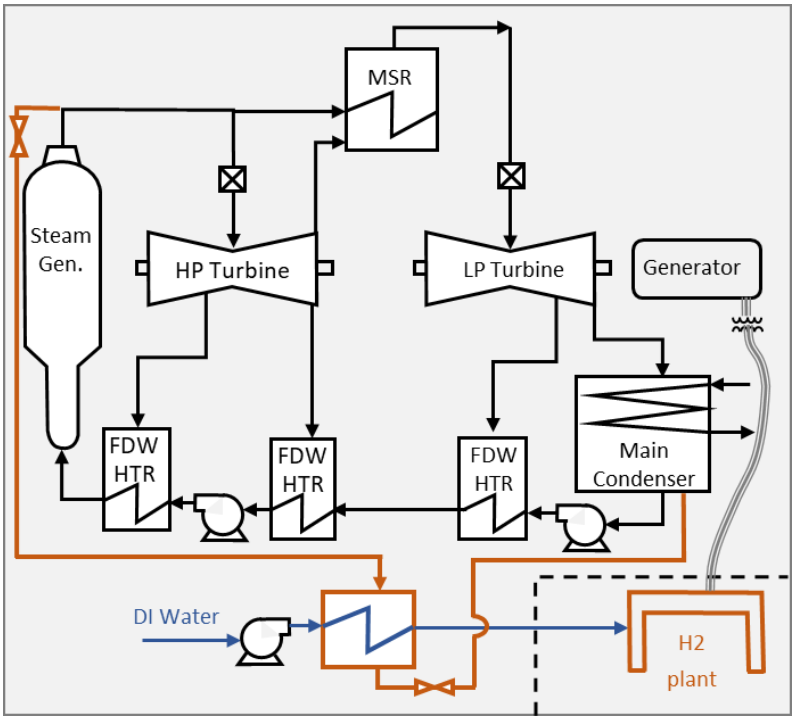

Figure 1-1. Simplified diagram of the PWR modified to dispatch thermal power to a high temperature electrolysis (HTE) hydrogen production plant.

Electric coupling to the bulk power grid and the hydrogen plant is accomplished by coupling the simulator to Digital Real Time Simulation (DRTS), which will provide the power systems models of the grid and hydrogen plant that can run in real time. The electrical load from the hydrogen plant is read as an input variable in the GPWR simulator and used to monitor the electrical power dispatch from the GPWR control room.

Section 2 describes electric power dispatch simulation options for coupled electric and thermal power dispatch from the RO-TPD-PWR simulator. Section 3 describes the model formulation, and Section 4 compares simulation results with those of prior published work for PWR plant. Section 5 briefly summarized operating and transition modes of the simulator, while Section 6 presents the results of select simulations. Section 7 summarizes conclusions from the work.

2. ELECTRICAL POWER DISPATCH

2.1 Electrical Power Dispatch Overview

Similar to the TPD-GPWR, two specific electric dispatch cases are considered. The first case is applicable for hydrogen plants that consume less than approximately 60 MWe and can be treated essentially as an additional house load for the nuclear power plant. The associated thermal power requirement would be less than 15 MWth, which is less than 1% of the total available thermal power. This scale would likely be considered a technology demonstration with relatively low safety risk to the PWR. The second case assumes that as much as 15% of the total available thermal power (2900 x 0.15 = 435 MWth) is extracted for use by multiple thermal energy users, including a hydrogen production plant. In this case, the hydrogen plant could be designed to consume as much as 795 MWe and 191 MWth. The remaining [435 – 191] = 244 MWth would be available to other thermal energy users. In this second case, the electric power dispatch is greater than can be supplied as a house load internal to the NPP, and the electrical connection between the PWR and the hydrogen plant must follow a "standard" industrial facility connection to a power plant in which the connection occurs after the high voltage transformer in the PWR switchyard.

2.2 Case #1: Electric Power Dispatch Less Than Approximately 60 MWe

Figure 2-1 shows a single-line diagram of the PWR-hydrogen plant electrical connection, assuming that the hydrogen plant can be treated as a house load for the PWR. The hydrogen plant will require a combination of AC and DC power. Approximately 90% of the total power requirement is needed as DC power at a voltage of 200-800 VDC, so the electric power from the PWR generator will need to be stepped down and converted to DC. Approximately 10% of the total power required by the hydrogen plant is needed as AC power to operate pumps and blowers and electric topping heaters. Figure 2-1 only shows a single power converter, but it is likely that this system will be replicated multiple times so that the hydrogen plant can be installed and operated as separate modules on the scale of 5-25 MW each. For this case, the electrical connection between the PWR and the hydrogen plant could be modeled in GSE's GPWR simulator. Figure 2-2 shows a single-line diagram of the GPWR power system and includes a line for the connection to the hydrogen plant. This figure does not show the needed power transformers and breakers, although these items would need to be modeled in the modified simulator. In this case, the hydrogen plant is powered from what would be a third unit auxiliary transformer (UAT).

A concern in this design is that in the event the hydrogen plant must be quickly isolated from the PWR, the power to the hydrogen plant would be diverted to the Generator Step-Up (GSU) transformer, which could actuate protective relays and potentially trip the main generator of the PWR. To avoid this unallowable event, the power being dispatched to the hydrogen plant must be very low relative to the total generator capability. Each of the UATs are rated at 67 MVA, and it is required that a single UAT be able to support all auxiliary loads, so in this design, electric dispatch to the hydrogen plant is limited to approximately 60 MWe.

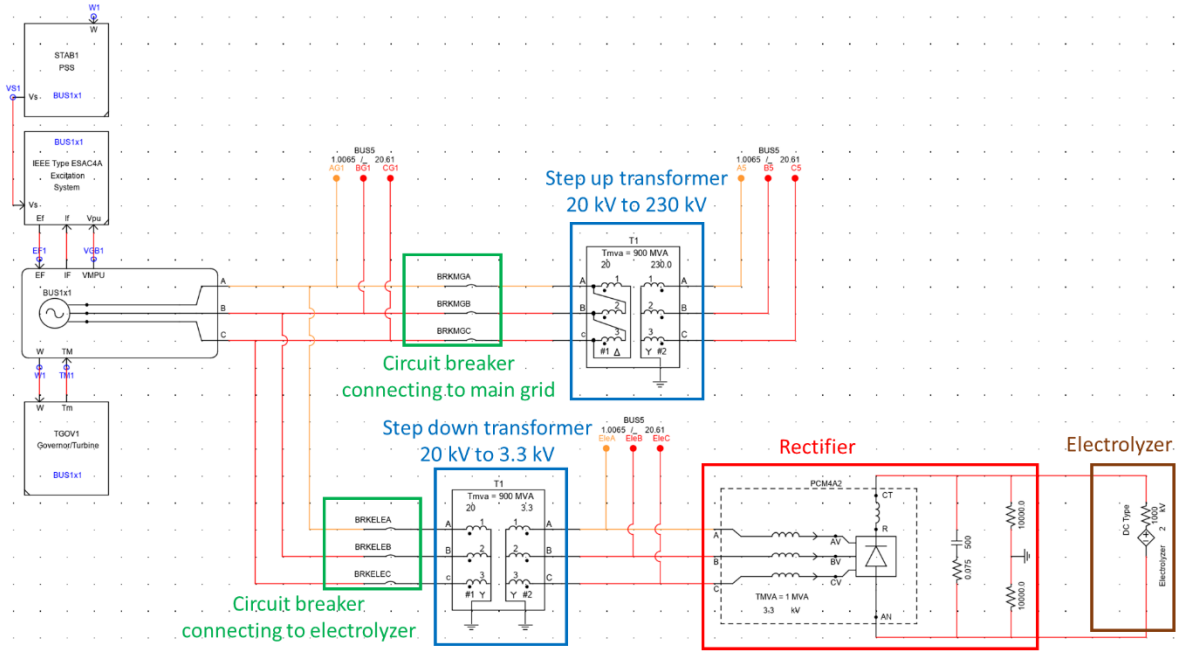

Figure 2-1. Single-line diagram of PWR-Hydrogen plant electric power connection for a demonstration-scale hydrogen production plant that is less than approximately 60 MWe.

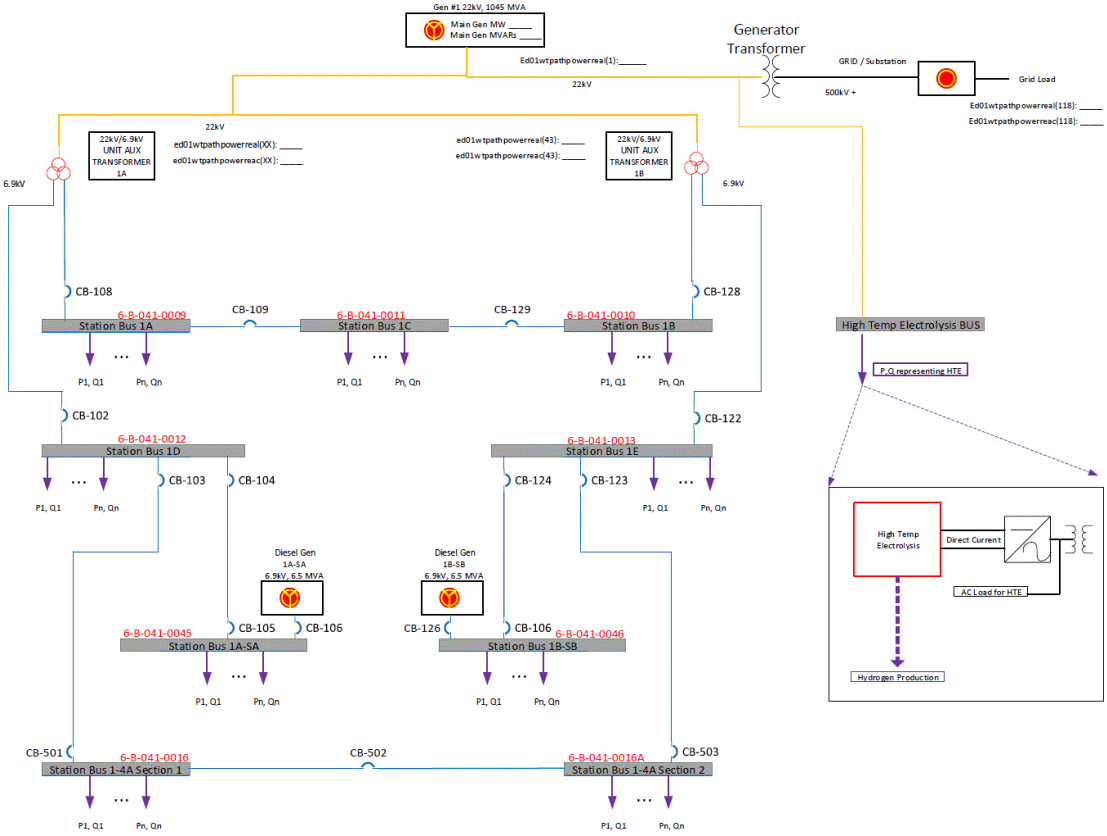

Figure 2-2. Single-line diagram of GSE's GPWR simulator, including a connection to a demonstration-scale hydrogen plant.

2.3 Case #2: Electric Power Dispatch Greater than Approximately 60 MWe

In this case, the connection of the hydrogen plant to the PWR will follow a standard industrial facility connection to a power plant in which the power connection is made on the high voltage side of the GSU. Transmission cables at switchyard voltage would carry power to the hydrogen plant approximately 1 km from the PWR. For large quantities of hydrogen production, the hydrogen plant must be located some distance (0.5-1.0 km) from the PWR to protect the PWR from potential hydrogen deflagration events. A sudden loss-of-load at the hydrogen plant would be similar to any nearby loss of load, and the impact to the generator would follow normal "generator load rejection" protection schemes and would be evaluated accordingly. As an example, General Electric (GE) generators have load rejection relaying that will trip the main generator on a 40% mismatch between reactor power and generator output. A notable issue for this case is the "Point of Interconnection" or POI that demarcates the equipment owned by the nuclear utility and the grid operator. There is interest to tap off the power line to the hydrogen plant after the GSU but before the POI, if possible, so that power can be supplied to the hydrogen plant without being subject to grid fees. This may be possible for plants in which the POI is at the first disconnect switch after the GSU going to the switchyard; however, it will likely not be possible for plants in which the POI is right at the connection to the HV bushing.

For the purposes of this report that focus on thermal power dispatch (TPD) of 15% and 50%, it is assumed that the coupled electric power dispatch will be greater than 60 MWe, so the electrical connection to the hydrogen plant will follow a standard industrial facility connection. Because the nuclear plant is coupled to the bulk power gird, simulating the impact of a sudden loss of load at the hydrogen plant will require a power systems simulation that includes the local power grid, the nuclear power plant, and the hydrogen plant, which may be separated into multiple modules. The power grid and the power systems of the hydrogen plants will be modeled using Real Time Digital Simulation (RTDS). For coupled electric and thermal power dispatch simulations involving the RO-TPD-PWR simulator, the instantaneous values of the generator's three-phase terminal voltages will be sent to RTDS through an ethernet connection that has been established between INL's Human Systems Simulation Laboratory (HSSL) and INL's Digital Real-Time Grid Simulation Laboratory. A controllable voltage source is modeled inside RTDS to leverage the voltage input from the RO-TPD-PWR. Instantaneous output voltage of the voltage source closely follows the value sent from the RO-TPD-PWR. The load on the electric grid simulated inside RTDS draws current from the voltage source, and the current value caused by the load is sent back to the RO-TPD-PWR for computing the electric-mechanical reaction inside the generator model.

3. PWR MODEL

3.1 Model Overview

As shown in Figure 3-1 and similar to a typical PWR, the model consists of a primary cycle and a secondary cycle. The primary cycle includes the reactor, steam generator (SG), and reactor coolant pump. The secondary cycle includes two high-pressure (HP) turbines, three low-pressure (LP) turbines, a moisture separator and reheater (MS/R), deaerator feed water heater, two HP feed water (HP-FW) heaters, and three LP feed water (PL-FW) heaters, a condenser, a condenser LP pump and an HP pump. The steam dump line from the main steam line to the condenser, as featured in typical PWRs, is also included in the model. However, an extraction heat exchanger is included in the turbine bypass (steam dump) line and it is relabeled the extraction steam line (XSL). The extraction heat exchanger uses heat from the main steam line to generate demineralized steam for hydrogen production. Two parameters are required to initialize the model. Those parameters are the reactor power (P_{th}) and the percentage of the

main steam extracted for thermal power dispatch (*%TPD*), which is defined as the ratio of mass flow in the XSL the mass flow in the main steam line ($\%TPD = \dot{m}_{XSL}/\dot{m}_1$). At standard operating conditions, the main steam pressure setpoint is determined by the reactor power. It is important to realize that the mass flow rate in the XSL impacts the temperature and pressure at the exit of the steam generator, and consequently the main steam flow rate ($\dot{m}_1$) must be calculated as part of the model initialization for the given reactor power and percent steam extraction to the XSL (*%TPD*).

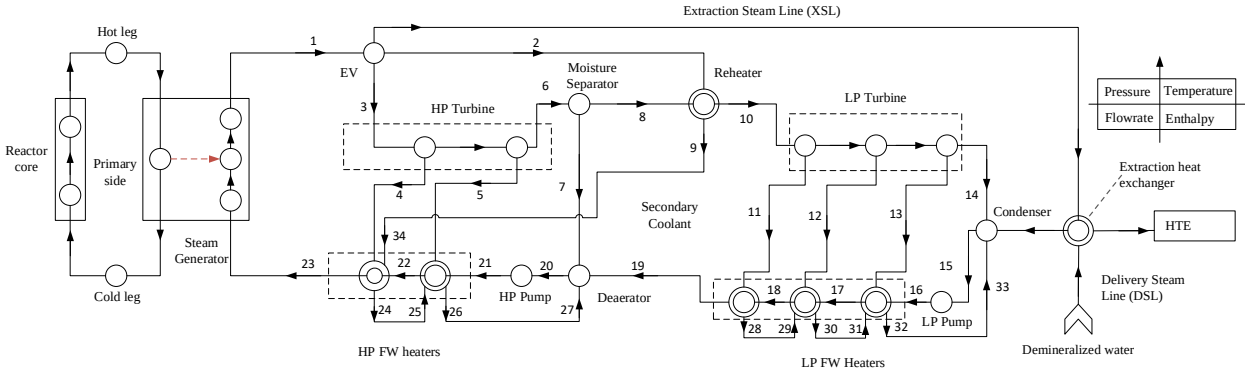

Figure 3-1. Diagram of the PWR modified to dispatch thermal power to a high temperature electrolysis (HTE) hydrogen production plant.

As noted above, the simulator is built on models that have been developed in previous work, including a Rancor Microworld model previously developed by INL and the University of Idaho [1]. The model of the secondary cycle of the RO-TPD-PWR simulator follows that developed by Ibrahim et al. [5]. The previous implementation of the Rancor model was implemented in the C# programming language for Microsoft's .NET Framework so that it could be easily used as part of a Windows Presentation Foundation (WPF) application. This version of the Rancor model is implemented in the Python programming language. It is broadly compatible with Python versions 3.6, 3.7, and 3.8 across Windows 10 (Anaconda, python.org), macOS (homebrew), and GNU/Linux (Ubuntu packages). The model requires NumPy, Matplotlib (for generating plots), iapws and pyXsteam. Rancor follows an object-oriented programming paradigm with a class for an SMR model and a class for a PWR with a secondary system that inherits the SMR class. A data historian is implemented as a third class that supports both the SMR and PWR models.

The model algorithm proceeds as follows:

i. Receive input parameters of reactor power (P_{th}) and percent steam extraction to the XSL (*%TPD*).

ii. Determine main steam pressure (p_1).

iii. Determine pressure at the inlets and outlets of as many components as possible.

iv. Calculate ratios of mass flow rates in the secondary cycle, including the XSL.

v. Determine thermodynamic properties, including pressure (*p*), temperature (*T*) entropy (*S*), enthalpy (*h*), and moisture content (*X*) at the inlets and outlets of all components.

vi. Calculate the feedwater flow rate to the steam generator ($\dot{m}_{23}$) required to maintain the main steam pressure at a given value based on the given reactor power level.

vii. Calculate the turbine work and heat consumed in producing demineralized steam for the hydrogen plant.

During calculations in which the PWR simulator is transitioned from one state to another, such as 0% steam extraction to 15% steam extraction, the proportional integral (PI) controller performs several key functions. First, the controller steps the setpoint for percent steam extraction (*%TPD*) to follow a linear ramp. Second, the controller adjusts the feedwater flow rate to the steam generator ($\dot{m}_{23}$) as needed maintain the temperature and pressure of the main steam (T_1 and p_1, respectively) constant for the given reactor power level. This control is necessary because the temperature of the feedwater entering the steam generator (T_{23}) depends upon the percent steam extraction (*%TPD*). This dependency arises due to two factors. First, the temperature of the condensate exiting the extraction heat exchanger is different than the temperature of condensate exiting the LP turbine ($\dot{m}_{14}$), and second, heat provided to the feedwater heaters comes from the turbine system and decreases as the percent steam extraction increases. The PI controller also operates the control rods based on the average primary coolant temperature and operates the LP and HP feedwater pumps to maintain constant pressure ratio compared to the main steam pressure, as described below.

3.2 Pressure Calculations

Steam exiting the steam generator is saturated, so that $T_1 = T_{sat}$, and $p_1 = p_{sat}$. We assume the pressure drop across valves is negligible, so that $p_1 = p_2 = p_3 = p_{XSL}$. To calculate the pressure throughout the remainder of the secondary cycle, it is assumed that the relative flow resistances of the turbine and feedwater lines remains unchanged. Thus, the ratios of flows through different lines and also the ratios of pressure drops do not change. This rather crude approximation has significant impact on the accuracy of the simulation predictions and will be revisited later. Assuming the ratios mass flows in the feedwater heater lines remains the same for different levels of thermal power extraction, the pressure of the steam extracted from the turbine units can be considered a ratio of the turbine inlet pressure:

$$p_i = a_i * p_3 \;\forall\, i \in \{4,5,6\}$$
$$p_i = a_i * p_{10} \;\forall\, i \in \{11,12,13,14\}. \qquad \text{Eq. (3.1)}$$

We further assume that at quasi-steady state, pressure drops across the moisture separator, reheater and deaerator are negligible, and also that pressure drops across the feedwater lines are negligible. With those approximation, $p_6 = p_7 = p_8 = p_9 = p_{10} = p_{16} = p_{17} = p_{18} = p_{19} = p_{20} = p_{27}$. Also, $p_{21} = p_{22} = p_{23}$. As noted above, the LP and HP pumps are controlled to maintain a constant pressure ratio with p_1. Combining that constrain with Eq. (1), we find that

$$p_i = a_i * p_1 \;\forall\, i \in \{16,21,34\}. \qquad \text{Eq. (3.2)}$$

3.3 Mass Flow Calculations

Steam exiting the steam generator is saturated, so that $T_1 = T_{sat}$, and $p_1 = p_{sat}$. We assume the pressure drop across valves is negligible, so that $p_1 = p_2 = p_3 = p_{XSL}$. Based on the approximation that the ratios of the flow resistances across the turbine and feedwater lines remains constant, the ratios of the flows through those lines also remains constant, and we have

$$\dot{m}_j = b_j * \dot{m}_1 \;\forall\, j \in \{\text{2-6, 11-14, 16-19, 21-23, 34}\}. \qquad \text{Eq. (3.3)}$$

In the moisture separator, only the vapor portion is passed to the LP turbine while the liquid portion is diverted to the deaerator. Also, the reheater is closed. Thus, the flowrates to the deaerator reheater are given as:

$$\dot{m}_7 = \dot{m}_6 * (1 - x_6) = b_6 * \dot{m}_1 * (1 - x_6) = b_7 * \dot{m}_1$$

$$\dot{m}_8 = \dot{m}_{10} = \dot{m}_6 * x_6 = b_6 * \dot{m}_1 * x_6 = b_8 * \dot{m}_1. \quad \text{Eq. (3.4)}$$

where x_6 is the void fraction of the two-phase mixture at the inlet of moisture separator. The ratios of the mass flow at points 7 and 8 compared to $\dot{m}_1$ (denoted by b_7 and b_8, respectively) can be defined in terms of x_6 and $\dot{m}_1$ as $b_7 = b_6 * (1 - x_6)$ and $b_8 = b_{10} = b_6 * x_6$. The steam arriving at the condenser is the sum of coolant returning from the third LP FW heater, the LP turbine, and the XSL, which is expressed as

$$\dot{m}_{15} = \dot{m}_{TPE} + \dot{m}_{14} + \dot{m}_{33} \quad \text{Eq. (3.5)}$$

where $\dot{m}_{33}$ is the sum of $\dot{m}_{11}, \dot{m}_{12}$ and $\dot{m}_{13}$.Therefore, $\dot{m}_{15}$ can be represented as a linear function of $\dot{m}_1$:

$$\dot{m}_{15} = \dot{m}_{TPE} + \dot{m}_{14} + \dot{m}_{11} + \dot{m}_{12} + \dot{m}_{13} = (b_{TPE} + b_{11} + b_{12} + b_{13} + b_{14}) * \dot{m}_1 = b_{15} * \dot{m}_1 \quad \text{Eq. (3.6)}$$

Since the feedwater heaters are closed, the steam flowing in the paths between condenser and the deaerator are equal, such that $\dot{m}_{16} = \dot{m}_{17} = \dot{m}_{18} = \dot{m}_{19} = \dot{m}_{15}$. The deaerator receives flow from moisture separator, LP main feedwater line and the second HP FW heater. Negligible vapor content is vented out to the atmosphere. Thus, the flow at the outlet of deaerator is given as

$$\dot{m}_{20} = x'_{20} * (\dot{m}_7 + \dot{m}_{19} + \dot{m}_{27}) = x'_{20} * (\dot{m}_7 + \dot{m}_{19} + \dot{m}_4 + \dot{m}_5). \quad \text{Eq. (3.7)}$$

where x'_{20} is the void fraction of the mixture inside the deaerator chamber and $\dot{m}_{27}$ is the sum of $\dot{m}_4$ and $\dot{m}_5$. x'_{20} is distinguished from x_{20}, which is the vapor fraction at the deaerator outlet and is equal to one because only liquid exits the outlet. Based on the above discussion, $\dot{m}_{27}$ can be represented as the function of $\dot{m}_1$:

$$\dot{m}_{20} = x_{20} * (b_7 + b_{19} + b_4 + b_5) * \dot{m}_1 = b_{20} * \dot{m}_1 \quad \text{Eq. (3.8)}$$

Similarly, the feedwater flow rates at different stages of secondary coolant circuit between the deaerator and the steam generator are given as $\dot{m}_{23} = \dot{m}_{22} = \dot{m}_{21} = \dot{m}_{20}$. From the analysis above, it is clear that all the flow rates in the secondary cycles are linear ratios of $\dot{m}_1$ and can be calculated as long as the void fractions in the moisture separator and deaerator are known (x_6 and x'_{20}, respectively).

3.4 Thermodynamic State Calculations

The steam supplied to the XSL, reheater and HP turbine inlet is a saturated vapor at the same temperature and pressure as the outlet of the steam generator. Based on the known pressure, the other thermodynamic state variables can be determined from steam tables as

$$x_k = 1 \ \forall \ k \in \{1, 2, 3, \text{XSL}\}$$
$$h_k, T_k, s_k = f_2(p_k, x_k) \ \forall \ k \in \{1, 2, 3, \text{XSL}\}. \quad \text{Eq. (3.9)}$$

where f_2 represents steam table reference functions based on saturated pressure and the void fraction. Approximating the turbines as isentropic, the other thermodynamic state variables can be determined from steam tables as

$$s_k = s_3 \ \forall \ k \in \{4, 5, 6\}$$
$$h_k, T_k, x_k = f_3(p_k, s_k) \ \forall \ k \in \{4, 5, 6\}\}. \quad \text{Eq. (3.10)}$$

where f_3 represents steam table reference functions based on pressure and entropy.

The reheater provides additional heat to the steam through closed-loop heat exchanger. It is assumed that all the latent heat of the extracted steam is used in the reheater.

$$\begin{gathered} \mathrm{x}_9 = 0 \\ \mathrm{h}_9, T_9, s_9 = f_2(p_9, x_9). \end{gathered} \quad \text{Eq. (3.11)}$$

The heat added to the main steam from the reheater is dependent on the steam flow, which is not yet known. However, the enthalpy at the outlet of reheater can be expressed as

$$\mathrm{h}_{10} = \frac{\dot{\mathrm{m}}_2 * (h_9 - h_2) + \dot{\mathrm{m}}_8 * h_8}{\dot{\mathrm{m}}_{10}}. \quad \text{Eq. (3.12)}$$

All mass flow rates are linear function of $\dot{\mathrm{m}}_1$. With the mass flow rate terms canceling in the above equations, the enthalpy at Node 10 can be formulated as:

$$\mathrm{h}_{10} = \frac{\mathrm{b}_2 * (h_9 - h_2) + \mathrm{b}_8 * h_8}{\mathrm{b}_{10}} \quad \text{Eq. (3.13)}$$

With the enthalpy and pressure known at the inlet of LP turbine, all other thermodynamic variables can be calculated using

$$T_{10}, s_{10}, x_{10} = f_4(p_{10}, h_{10}), \quad \text{Eq. (3.14)}$$

where f_4 represents steam table reference functions based on pressure and enthalpy.

Continuing with the assumption of isentropic processes in the LP turbine, the thermodynamic states of nodes in the LP feedwater heater lines can be calculated using the pressure and entropy:

$$\begin{gathered} s_k = s_{10} \ \forall \, k \in \{11,12,13,14\} \\ \mathrm{h}_k, T_k, x_k = f_3(p_k, s_k) \ \forall \, k \in \{11,12,13,14\}. \end{gathered} \quad \text{Eq. (3.15)}$$

The condenser outlet is saturated liquid, so that the remainder of the values at condenser outlet are calculated as

$$\begin{gathered} \mathrm{x}_{15} = 0 \\ \mathrm{h}_{15}, T_{15}, s_{15} = f_2(p_{15}, x_{15}). \end{gathered} \quad \text{Eq. (3.16)}$$

Assuming isentropic compression, the thermodynamic state variables for LP pump outlet can be determined as:

$$\begin{gathered} s_{16} = s_{15} \\ \mathrm{h}_{16}, T_{16}, x_{16} = f_3(p_{16}, s_{16}). \end{gathered} \quad \text{Eq. (3.17)}$$

The LP feedwater heaters receive the heat from the steam extracted from LP, such that the enthalpy of the feedwater at the outlet of first LP feedwater heater can be expressed as

$$\mathrm{h}_{19} = \frac{\dot{\mathrm{m}}_{11} * (h_{11} - h_{32}) + \dot{\mathrm{m}}_{12} * (h_{12} - h_{32}) + \dot{\mathrm{m}}_{13} * (h_{13} - h_{32}) + \dot{\mathrm{m}}_{16} * h_{16}}{\dot{\mathrm{m}}_{19}}. \quad \text{Eq. (3.18)}$$

As before, all mass flow rates in Equation 3.17 are linear function of $\dot{\mathrm{m}}_1$., such that $\dot{\mathrm{m}}_1$ can be canceled to obtain

$$\mathrm{h}_{19} = \frac{\mathrm{b}_{11} * (h_{11} - h_{32}) + \mathrm{b}_{12} * (h_{12} - h_{32}) + \mathrm{b}_{13} * (h_{13} - h_{32}) + \mathrm{b}_{16} * h_{16}}{\mathrm{b}_{19}}. \quad \text{Eq. (3.19)}$$

With enthalpy and pressure known all other thermodynamic variables can be calculated as:

$$T_{19}, s_{19}, x_{19} \;=\; f_4(p_{19}, h_{19})$$

The deaerator mixes the steam from three different paths: saturated liquid from the moisture separator, preheated feedwater coming from the LP feedwater heaters and the liquid coming from the heating loop of the HP feedwater heater. The enthalpy of the mixture inside the deaerator chamber can be written

$$\mathrm{h'}_{20} = \frac{\dot{\mathrm{m}}_{19} * h_{19} + \dot{\mathrm{m}}_7 * h_7 + \dot{\mathrm{m}}_{27} * h_{16}}{\dot{\mathrm{m}}_{19} + \dot{\mathrm{m}}_7 + \dot{\mathrm{m}}_{27}}. \qquad \text{Eq. (3.20)}$$

Replacing mass flowrates with a linear function of $\dot{\mathrm{m}}_1$ and canceling common $\dot{\mathrm{m}}_1$ terms, the enthalpy in Equation 3.20 can be expressed as

$$\mathrm{h}'_{20} = \frac{\mathrm{b}_{19} * h_{19} + \mathrm{b}_7 * h_7 + \mathrm{b}_{27} * h_{16}}{\mathrm{b}_{19} + \mathrm{b}_7 + b_{27}}. \qquad \text{Eq. (3.21)}$$

It should be noted here that the deaerator removes any vapor left in this mixture. Therefore, it is necessary to check if the mixture is in the saturation zone. The void fraction inside the deaerator is given as:

$$x'_{20} = f_5(p_{20}, h'_{20}. \qquad \text{Eq. (3.22)}$$

where f_5 represents steam table reference functions based on pressure and enthalpy. The enthalpy at deaerator outlet is given as:

$$h_{20} = \begin{cases} f_6(p_{20}, 0)\,, & x'_{20} > 0 \\ h'_{20}\,, & otherwise \end{cases}. \qquad \text{Eq. (3.23)}$$

where f_6 represents steam table reference functions based on pressure and void fraction. The remainder of the variables at the deaerator output are calculated as:

$$T_{20}, s_{20}, x_{20} \;=\; f_4(p_{20}, h_{20}). \qquad \text{Eq. (3.24)}$$

Assuming isentropic compression, the thermodynamic state of the outlet of the HP pump is given as

$$\begin{aligned} s_{21} \;&=\; s_{20} \\ \mathrm{h}_{21}, T_{21}, x_{21} \;&=\; f_3(p_{21}, s_{21}). \end{aligned} \qquad \text{Eq. (3.25)}$$

The HP feedwater heaters receive heat from HP turbine. The enthalpy of the feedwater at the outlet of first HP feedwater heater or the inlet of steam generator is given by

$$\mathrm{h}_{23} = \frac{\dot{\mathrm{m}}_9 * (h_9 - h_{26}) + \dot{\mathrm{m}}_4 * (h_4 - h_{26}) + \dot{\mathrm{m}}_5 * (h_5 - h_{26}) + \dot{\mathrm{m}}_{21} * h_{21}}{\dot{\mathrm{m}}_{23}}. \qquad \text{Eq. (3.26)}$$

As before, all mass flow rates in Equation 3.26 are linear function of $\dot{\mathrm{m}}_1$, so that Eq. 3.26 can be simplified to

$$\mathrm{h}_{23} = \frac{\mathrm{b}_9 * (h_9 - h_{26}) + \mathrm{b}_4 * (h_4 - h_{26}) + \mathrm{b}_5 * (h_5 - h_{26}) + \mathrm{b}_{21} * h_{21}}{\mathrm{b}_{23}}. \qquad \text{Eq. (3.27)}$$

With enthalpy and pressure known, all other thermodynamic variables can be calculated as:

$$T_{23}, s_{23}, x_{23} = f_4(p_{23}, h_{23}). \quad \text{Eq. (3.28)}$$

3.5 Absolute Mass Flow and Turbine Power Calculations

With the thermodynamic state of the feedwater at steam generator inlet known, steam flow required to maintain the steam generator outlet at the rated operating condition is calculated as:

$$\dot{m}_1 = \frac{P_{th}}{h_1 - h_{23} * b_{23}}. \quad \text{Eq. (3.29)}$$

Having finally determined the value of $\dot{m}_1$, the remaining the flow rates can be calculated using equations 3.1 to 3.8. The mechanical power output of the HP and LP turbines is given by

$$P_m^{HPT} = \eta_{\mathrm{HPT}}(\dot{m}_3 * (h_3 - h_4) + (\dot{m}_3 - \dot{m}_4)(h_4 - h_5) + (\dot{m}_3 - \dot{m}_4 - \dot{m}_5)(h_5 - h_6))$$
$$P_m^{LPT} = \eta_{\mathrm{LPT}}\big((\dot{m}_{10} * (h_{10} - h_{11}) + (\dot{m}_{10} - \dot{m}_{11})(h_{11} - h_{12}) + (\dot{m}_{10} - \dot{m}_{11} - \dot{m}_{12})(h_{12} - h_{13}) + (\dot{m}_{10} - \dot{m}_{11} - \dot{m}_{12} - \dot{m}_{13})(h_{13} - h_{14})\big).$$

Eq. (3.30)

The total mechanical power output of the LP turbines is given by $P_m = P_m^{HPT} + P_m^{LPT}$.

3.6 Thermal Power Extraction Calculations

The extraction steal line (XSL) is simplified with a heat exchanger transferring the heat from the XSL to the industrial heat user. The assumption is that the extraction heat exchanger will extract all the latent heat from the steam in XSL and send the condensed liquid to the condenser. Assuming isobaric heat extraction from the XSL,

$$p_{XSL}^{out} = p_{XSL}^{in} \quad and \quad x_{XSL}^{out} = 0$$

$$h_{XSL}^{out}, T_{XSL}^{out}, s_{XSL}^{out} = f_2(p_{XSL}^{out}, x_{XSL}^{out}). \quad \text{Eq. (3.31)}$$

With the steam condition known for the inlet of XSL, the heat extracted by heat exchanger can be calculated using 3.31.

3.7 Reactor Model

The reactor core and steam generator models follow the approach described by Poudel and Gokarjau [2]. The description below follows that given in [2]. In brief, the reactor core model captures the neutron dynamics within the core, as well as the thermal hydraulics and convection heat transfer in the primary system. The reactor core model assumes that the pressure in the reactor pressure vessel (RPV) is constant to simplify the simulation. This assumption is valid inasmuch as the primary system is not subjected to any dramatic transients during simulations, which is consistent with the key objective of the modeling to maintain the primary system at nearly steady state while flexing the secondary system.

Core neutronics is approximated as the average neutron flux from a lumped kinetics model that includes a single energy model and a neutron precursor group that includes six groups of delayed neutrons.

$$\frac{d\phi}{dt} = \frac{\rho}{\Lambda} - \frac{\beta}{\Lambda}\phi + \lambda C$$
$$\frac{dC}{dt} = \frac{\beta}{\Lambda}\phi - \lambda C$$

Eq. (3.33)

The net core reactivity (ρ) is determined as the total contribution of reactivities from fuel and moderator temperature feedbacks and control rod operation.

$$\rho = \rho_{ext} + \alpha_f \Delta T_f + 0.5\alpha_c(\Delta T_{c1} + \Delta T_{c2}) \quad \text{Eq. (3.34)}$$

The heat transfer between the fuel lumps and primary coolant is estimated using Mann's model [6]. Within the core region, primary coolant is represented by two nodes. The behavior of fuel and primary coolant temperatures are given by

$$\frac{dT_f}{dt} = [\tau P_0 \phi + h_{fc} A_{fc}(T_{c1} - T_f)]/m_f c_{pf}$$
$$\frac{dT_{c1}}{dt} = [(1-\tau)P_0\phi + h_{fc}A_{fc}(T_f - T_{c1})]/m_c c_{pc} + 2\dot{m}_{cp}(T_{c1} - T_{c2})/m_c$$
$$\frac{dT_{c2}}{dt} = [(1-\tau)P_0\phi + h_{fc}A_{fc}(T_f - T_{c1})]/m_c c_{pc} + 2\dot{m}_{cp}(T_{CL} - T_{c1})/m_c$$

Eq. (3.35)

The primary coolant flow could be either passive or active. If active, primary coolant flow is regulated using recirculation pump as needed. If passive, the temperature difference between hot leg and cold leg creates a natural buoyancy force to vertically carry the coolant through the reactor core.

$$\dot{m}_{NC} = \dot{m}_{NC}^r \sqrt[3]{(P_{th}^r)/P_{th}}$$
$$\dot{m}_{cp} = \begin{cases} \dot{m}_{pump}, & active\ circulation \\ \dot{m}_{NC}, & passive\ circulation \end{cases}$$

Eq. (3.36)

The mean temperatures of the hot and cold leg regions is approximated to first-order with linear functions

$$\frac{dT_{HL}}{dt} = \frac{T_{c2} - T_{HL}}{\tau_{HL}}, \frac{dT_{CL}}{dt} = \frac{2T_P - T_{HL} - T_{CL}}{\tau_{CL}}$$

Eq. (3.37)

where $\tau_{HL} = m_{HL}/\dot{m}_{cp}$ and $\tau_{CL} = m_{CL}/\dot{m}_{cp}$.

3.8 Steam Generator Model

The steam generator is represented using the simplified three-lump model advocated by Robinson [7]. In this approach, the primary coolant, tube metal, and secondary coolant are modeled as separate lumped masses with temperatures T_p, T_m, and T_{sat}. Heat transfer between the fluids and metal is calculated using the average temperature of each lumped mass. The secondary coolant enters the steam generator in a saturated state with pressure p_{sat} from the feedwater heaters and exits the steam generator as saturated vapor. The thermodynamics of the steam generator are governed by

$$\frac{dT_p}{dt} = K_{HL}(T_{HL} - T_p) + K_m(T_m - T_p)$$

$$\frac{dT_m}{dt} = K_{mp}(T_P - T_m) + K_{ms}(T_1 - T_m)$$

$$\frac{dP_1}{dt} = K_{sm}(T_m - T_1) - \dot{m}_{cs}\left(U_v - C_{pi}T_{23}\right). \qquad \text{Eq. (3.38)}$$

where $K_{HL} = \dot{m}_{cp} m_p^{-1}$, $K_m = h_{pm} A_{pm} m_p^{-1} c_p^{-1}$, $K_{mp} = h_{pm} A_{pm} m_m^{-1} c_m^{-1}$, $K_{ms} = h_{ms} A_{ps} m_m^{-1} c_m^{-1}$, $K_{sm} = h_{ms} A_{ps} m_m$, $K_s = m_{sw} \frac{dU_w}{dp} + m_{sv} \frac{dU_v}{dp} - m_{sv} U_{wv} v_{wv}^{-1} \frac{dv_g}{dp}$, $U_{wv}=U_v-U_w$, *and* $v_{wv}=v_v-v_w$.

3.9 Primary Coolant Initialization

Sections 3.2 to 3.6 discussed the initialization of the secondary coolant circuit for a given initial condition (P_{th} and *%TPD*). This section uses the values calculated for the secondary side to initialize the reactor primary side. The term $U_v - C_{pi}T_1$ in Eq. 3.38 is the difference of internal energy of the vapor and feedwater across the steam generator secondary line. Considering isobaric heat addition at the steam generator, the internal energy gained by the feedwater is same as the change in enthalpy:

$$U_v - C_{pi}T_{23} = h_1 - h_{23}$$

Rewriting the third equation in Eq. 3.38 for a steady state condition (the derivative equals zero):

$$T_m = \frac{\dot{m}_{cs} * (h_1 - h_{23})}{k_{sm}} + T_{sat}. \qquad \text{Eq. (3.39)}$$

With the values on the right side of the Equation 3.39 known from the secondary side calculations, T_m can be calculated for a given initial condition.

Rewriting first and second equation in Eq 3.38 for a steady state condition, the values of T_p and T_{HL} can be calculated as:

$$T_p = \frac{K_{ms} * (T_m - T_1)}{k_{mp}} + T_m$$

$$T_{HL} = \frac{K_m * (T_p - T_m)}{k_{HL}} + T_p. \qquad \text{Eq. (3.40)}$$

4. Comparison of Simulator Predictions Without Thermal Power Dispatch (TPD) to Literature Steady-State PWR Simulation

The previous implementation of Rancor was primarily intended as a real-time simulation model for human-in-the-loop simulations to examine human performance and reliability. The model implementation consisted of a single-phase primary side and a simplified secondary side with an infinite feedwater source and condenser sink. The reactor model conserved mass and energy but did not include reactor neutronics. The current implementation (RO-TPD-PWR) described in this report is developed to be a more accurate representation that can be used for engineering purposes as well as human-in-the-loop testing.

As previously described, the secondary system was modeled after Ibrahim et al. [5] and the node numbering in Figure 1-1 is consistent with that of Ibrahim et al. [5] as shown in Figure 4-1 allowing for direct comparisons between node states. Table 4-1 presents the thermodynamic data for the RO-TPD-PWR secondary model with no thermal power dispatch (0% TPD). Results from the RO-TPD-PWR simulator are within 1% most of the nodes in Ibrahim et al. model, except for a few exceptions. Larger discrepancies between the models are depicted in Table 4-2. The large discrepancies in mass flow for

node 34 and nodes 24-27 are due to the mass flows not being properly conserved with the Ibrahim et al. model. The first HP feedwater heater receives steam from the first stage of the HP turbine and the reheater. The mass flow exiting the first HP feedwater heater at node 24 should be the sum of these two flows (Nodes 4, 9). Nodes 25-27 are downstream of Node 24, which is why the mass flows are different between the two models. In this instance, the Ibrahim et al. model fails to conserve mass, and the RO-TPD-PWR simulator corrects this error.

The discrepancy for Node 20 is also explained by the Ibrahim et al. model failing to conserve mass, in this instance from the suction of the HP feedwater pump to the outlet. Assuming the level in the deaerator remains constant the mass flow for Node 20 should be the sum of Nodes 7, 19, and 27.

In the RO-TPD-PWR simulator, the feedwater temperatures/enthalpies through Nodes 20-23 are slightly lower than in the Ibrahim et al. mode because that model assumes the dearerator outlet pressure and enthalpy (and therefore temperature) is condensed from the moisture separator (Node 7). However, the dearator also receives flow from the shell side of the LP feedwater heaters and tube side of the HP feedwater heaters. In the RO-TPD-PWR simulator, the enthalpy of the HP feedwater pump inlet (Node 20) is determined by energy balance from all three dearator inlets before determining temperature and entropy. This between the models also impacts Nodes 21, 22, and 23 because they are downstream of Node 20. Lastly, in the RO-TPD-PWR simulator, the enthalpies, entropies, and steam qualities show small discrepancies for the LP turbine outlet stages (Nodes 11, 12, 13, 14) due to treating the LP turbine as isentropic.

In summary, the discrepancies between the two models are explained, and the RO-TPD-PWR simulator appears to reasonably model the steady state response of a PWR secondary system.

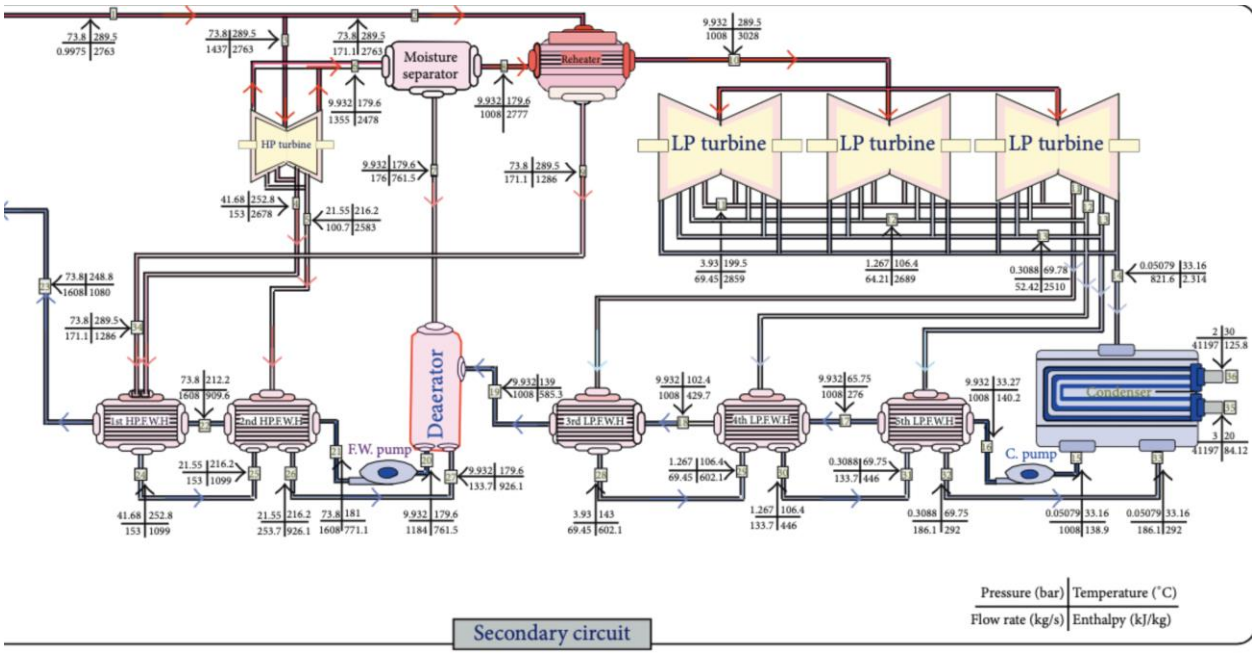

Figure 4-1. PWR node numbering and diagram from Ibrahim, Ibrahim and Sami [5].

Table 4-1. Thermodynamic data for the RO-TPD-PWR simulation secondary system. %TPD = 0.

Node	**Name**	**T**	**P**	**h**	**s**	**x**	**ṁ**
		°C	MPa	kJ/kg	kJ/kg·k		kg/s
1	gv	289	7.34	2768	5.790	1.000	2373
2	ms_reheater	289	7.34	2768	5.790	1.000	252
3	hpt	289	7.34	2768	5.790	1.000	2120
4	hpt_stg1	252	4.15	2661	5.790	0.918	226
5	hpt_stg2	216	2.14	2544	5.790	0.863	149
6	hpt_stg3	179	0.99	2415	5.790	0.821	1746
7	deaerator	179	0.99	760	2.133	0.000	313
8	reheater	179	0.99	2777	6.589	1.000	1433
9	reheater_hpfwh1	289	7.34	1285	3.152	0.000	252
10	lpt	293	0.99	3038	7.106	1.000	1433
11	lpt_stg1	183	0.39	2825	7.106	1.000	99
12	lpt_stg2	106	0.13	2619	7.106	0.970	91
13	lpt_stg3	70	0.03	2401	7.106	0.904	75
14	lpt_stg4	33	0.01	2168	7.106	0.838	1168
15	cond_mix	33	0.01	139	0.479	0.000	1433
16	cpump	33	0.99	140	0.479	0.000	1433
17	lpfwh3	64	0.99	270	0.884	0.000	1433
18	lpfwh2	100	0.99	419	1.304	0.000	1433
19	lpfwh1	136	0.99	572	1.696	0.000	1433
20	fwpump_suction	163	0.99	690	1.976	0.000	2373
21	fwpump	164	7.34	697	1.976	0.000	2373
22	hpfwh2	195	7.34	833	2.277	0.000	2373
23	hpfwh1	232	7.34	1002	2.623	0.000	2373
24	hpfwh1_stm_out	252	4.15	1098	2.816	0.000	478
25	hpfwh2_stm2	216	2.14	1098	2.834	0.092	478
26	hpfwh2_stm_out	216	2.14	925	2.480	0.000	627
27	deaerator_hpfwh_stm	179	0.99	925	2.497	0.082	627
28	lpfwh1_stm_out	143	0.39	601	1.768	0.000	99
29	lpfwh2_stm2	106	0.13	601	1.787	0.070	99
30	lpfwh2_stm_out	106	0.13	445	1.377	0.000	190
31	lpfwh3_stm2	70	0.03	445	1.399	0.066	190
32	lpfwh3_stm_out	70	0.03	291	0.951	0.000	265
33	cond_fw	33	0.01	291	0.978	0.063	265
34	hpfwh1_stm2	252	4.15	1285	3.172	0.110	252

Table 4-2. Comparison between temperatures (T), pressures (P), enthalpies (h), moisture contents (x) and mass flow rates ($\dot{m}$) predicted by the RO-TPD-PWR simulator and results reported by [5]. Nodes with insignificant errors (<4%) are omitted.

Node	T	P	h	s	x	$\dot{m}$
7	0%	-1%	0%	0%	0%	21%
11	-8%	-1%	-1%	-1%	0%	-4%
12	0%	-1%	-3%	-2%	-3%	-4%
13	0%	-1%	-4%	-4%	-5%	-4%
14	0%	-1%	-6%	-6%	-6%	-4%
17	-2%	-1%	-2%	-2%	0%	-4%
18	-3%	-1%	-3%	-2%	0%	-4%
19	-2%	-1%	-2%	-2%	0%	-4%
20	-9%	-1%	-9%	-8%	0%	36%
21	-9%	-1%	-10%	-8%	0%	0%
22	-8%	-1%	-8%	-7%	0%	0%
23	-7%	-1%	-7%	-5%	0%	0%
24	0%	-1%	0%	0%	0%	112%
25	0%	-1%	0%	0%	0%	112%
26	0%	-1%	0%	0%	0%	67%
27	0%	-1%	0%	0%	0%	218%

5. Reduced-Order Thermal Power Dispatch (RO-TPD) PWR Simulation Operating and Transition Modes

5.1 Overview of Operation and Transition Modes

This section explains the operating and transition modes for the RO-TPD-PWR simulator. The principal operating thermal power dispatch modes of the integrated nuclear/hydrogen system include:

A. **Cold Shutdown** – the extraction steam line (XSL) has zero flow and is at ambient temperature.

B. **Hot Standby** – the XSL has minimal flow to maintain hot conditions at the hydrogen plant.

C. **Thermal Power Dispatch (TPD)** – the XSL has sufficient flow to provide the desired thermal power to the industrial process.

The discussion below focuses on the transition between Hot Standby and Thermal Power Dispatch (TPD) because that transition is the one that will be performed the most frequently in short time intervals and also has the highest risk for unexpected events. It is worth noting that the TPD required to maintain hot standby is expected to be about 5% of the maximum TPD amount, so the infrequent transition from Cold Shutdown (0% TPD) to Hot Standby does not represent a significant challenge to NPP operations.

Initial conditions are established in the simulator that correspond to each principal operating mode, so that the test procedures involve transitioning from one operating mode to another to understand how both the operator and the power plant respond to operational changes. Each operating mode refers to operation of the extraction steam line (XSL) and has little impact on the primary system of the PWR because the

reactor operates at approximately 100% thermal power generation for all standard operating modes of the TPD system. A key goal of the RO-TPD-PWR simulator is to enable operator tests with physical hardware that is controlled in a manner that is relevant to full-scale operations at nuclear power plants. The RO-TPD-PWR simulator provides the supervisory guidance to the operators to enable the pilot-scale equipment to mimic industrial-scale operations at a full-scale PWR. By including operators, hardware and simulation in a single test, assumptions and idealized conditions in full-scope, high-fidelity PWR simulators can be tested. For example, flow and pressure measurements in real pipes have uncertainty and fluctuations that may not be captured by computer simulations. Similarly, the behavior of real valves, actuators, and pumps can be different than that of idealized simulations. Physical tests with human operators and real valves, lines and heat exchangers assist understanding how to safely maintain the NPP at near 100% thermal power output while transitioning between TPD operating modes.

5.2 Procedure to Transition from Cold Shutdown to Hot Standby

The turbine load needs to be decreased before the TPD system is placed in Hot Standby and then the XSL control valve can be slowly opened. The procedural steps are:

1. Decrease the turbine load to the hot standby setpoint at a ramp rate of 5 MW/min (920 MW, 895 MW).
2. Slowly open the XSL control valve using a linear ramp rate to initiate pressurization of the TPD system. Do not let the XSL steam flow rate exceed the hot standby setpoint (27 lb/sec).
3. Monitor the XSL as it slowly pressurizes.

5.3 Procedures to Transition between Hot Standby and Thermal Power Dispatch (TPD)

The high-level steps to transition from Hot Standby to TPD are given below. The set points for 15% and 50% TPD are shown in parenthesis following the appropriate steps.

1. Prepare the turbine system for the ramp down in power by inputting the specified ramp rate (12 MW/min, 20 MW/min).
2. Input the turbine load setpoint and place the system into “GO” (705 MW, 320 MW).
3. Monitor the reactor power and prepare to open the XSL valve as the turbine power decreases.
4. Maintain the reactor power around 99% controlling the steam flow through the XSL system using the XSL control valve.
5. Reactor power should be maintained between 98.5% and 99.5% to avoid the risk of reactor overpower during the transient and the prevent movement of the control rods caused by the T_{ref} to T_{avg} mismatch.
6. Adjust the XSL flow set point to the XSL setpoint (537.9 lb/sec, 1793.0 lb/sec).
7. When the turbine control system reaches the power set point, continue to open the XSL flow valve until the set point is reached.
8. Thermal Power Dispatch (TPD) mode has been achieved.

The procedure to return to Hot Standby from TPD mode follows the same pattern in reverse order:

1. Prepare the turbine system for the ramp up in power by inputting the specified ramp rate (12 MW/min, 20 MW/min).
2. Ramp the XSL flow control valve to the closed position until a reactor power of 99% has been achieved.
3. Input the turbine load setpoint and place the system into “GO” (920 MW, 895 MW).

4. Maintain the reactor power between 98.5% and 99.5% by decreasing the steam flow rate in the XSL system.
5. Adjust the XSL controller set point to the Hot Standby value (27.0 lb/sec, 90.0 lb/sec).
6. Hot Standby mode has been achieved.

6. Reduced-Order Thermal Power Dispatch (RO-TPD) PWR Simulation Results

As noted above, simulations were performed for 15% and 50% thermal power dispatch (*%TPD* = 15% and 50%, respectively). The predicted response of the reactor power as steam flow is increased in the XSL is shown in Figure 6-1. To simplify the presentation of the results, the reactor power was not first decreased to 98.5% prior to initiating flow in the XSL. Increasing steam flow rate in the XSL is perceived by the reactor as an increase in turbine power demand and, consequently, causes an increase in reactor power. For 15% TPD, the increase in reactor power is less than 0.5%, while for 50% TPD, the increase in reactor power is greater than 1%. This undesirable result can easily be avoided by reducing the reactor power to 98.5% prior initiating flow in the XSL. Once the flow in the XSL stabilizes, the reactor power returns to 100%. As flow is decreased in the XSL to stop TPD operation, the reactor power responds by decreasing just as it would for a decrease in turbine power demand. The relationship between reactor power and ramping of flow in the XSL line can be modified by the T_{ref} and T_{ave} calculations as described in a prior report [3]. The values of these parameters during the simulations is shown in Appendix A. Modifying the calculation of these parameters will be the subject of future research using the full-scope TPD-GPWR simulator.

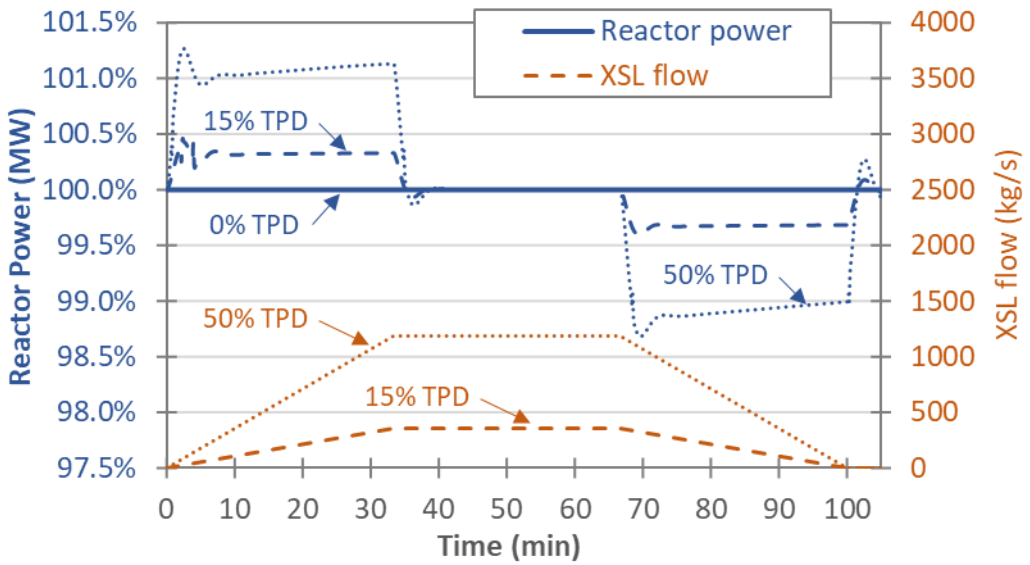

Figure 6-1. Predicted reactor power as a function of steam flow in the XSL for 0%, 15%, and 50% TPD.

Figure 6-2 shows predicted steady-state values of steam mass flow in the main steam line and the turbine system for 0%, 15%, and 50% TPD. Prediction results are compared with those from the full-scope TPD GPWR simulator (labeled as "Hancock, et al." [4]) and also with those of Ibrahim et al. for 0% TPD. Results from two different versions of the RO-TPD-GPWR simulator are shown in Figure 6-2. The results labeled "RO, linear" were obtained using the simulator model formulated as described above in Sections 3 and 4. In the second version of the simulator, labeled "RO, nonlinear," the assumption of

fixed ratios of flow rates in the feedwater lines was relaxed, based on the observation in prior work using a full-scope PWR simulator that the mass flow rates of steam in the feedwater heaters were impacted unevenly due to the addition of the thermal power dispatch (TPD) system [4]. Referring to Fig. 3-1, there are obvious reasons why the steam flow rates in the feedwater heaters are expected to be impacted unevenly. The approximation of fixed ratios of flow rates in the lines is only approximately valid for select conditions. Under laminar flow conditions, pressure drop in pipes is linearly proportional to volumetric flow rate, while for turbulent flow conditions, pressure drop increases approximately with the square of the volumetric flow rate. Pressure drop also increases with increasing fluid viscosity, such as due to changes in moisture content (steam quality). The turbine control system, which uses governor valves to regulate flow and pressure in the HP and LP turbines also impacts the flow rates in the feedwater heaters. Fluid flow within the turbines is highly complex with nonuniform steam quality, temperature, and pressure, such that the mass flow rate of steam extracted at different points in the turbine system for the feedwater heaters is expected to exhibit nonlinear behavior. The T-S and P-h diagrams for the turbines, which are included in Appendix A, show the variations those parameters in the turbine system and further support that flow from the extraction points in the turbine system will be unevenly impacted by changes in the fluid flow rate through the turbine system. For the second version of RO-TPD-PWR similar, the mass flow rates in the feedwater heaters were adjusted to approximately mimic the flow rates predicted by the full-scope TPD-GPWR simulator for similar conditions, based on results published in [4].

As noted above in Section 3.1, the temperature of the feedwater entering the steam generator (Node 23 in Figure 3-1) depends upon the steam flow in the XSL because increasing flow in the XSL removes steam from the turbine system that supports the feedwater heaters. The decrease the feedwater temperature entering the steam generator causes a decrease of steam flow in the main steam line because the heat from the reactor is steady. The decrease in steam flow through the main steam line and turbine system with increasing steam flow in the XSL is evident in Figure 6-2. The nonlinear version of the RO-TPD-PWR simulator, which more accurately accounts for steam flow impacts in the feedwater heaters, shows better agreement to predictions of steam flow in the main steam line obtained from the full-scope TPD-GPWR simulator (Hancock, et al.) than does the version of the RO-TPD-PWR simulator that assumes the ratios of flows in the feedwater heaters is fixed, regardless of flow in the XSL (labelled “RO, linear” in Figure 6-2). In fact, for both 15% and 50% TPD, the error of the “RO, nonlinear” model for main steam flow is less than half that of the “RO, linear” model, compared to results from Hancock, et al. Interestingly, however, the predictions of steam flow in the turbine system from the “RO, nonlinear” model appear to be somewhat poorer than those of the “RO, linear” model. The differences, however, are moderate, and the discrepancies between all turbine steam flow predictions are less than 10% of the full turbine steam flow.

As expected, the power extracted from the turbine system decreases as steam flow to the turbine system decreases and steam flow to the XSL increases. Figure 6-3 shows the predicted percent decrease in turbine power output for 15% and 50% TPD based on the full-scope TPD-GPWR simulator (“Hancock, et al.) and the two versions of the RO-TPD-PWR simulator. Predictions of turbine power output from the nonlinear version of the RO-TPD-PWR simulator most closely match those of the full-scope TPD-GPWR simulator, although discrepancies from both models are less than 7% of the full turbine power output. Figure 6-4 shows the predicted decrease in the feedwater entering the steam generator from the same simulations as featured in Figure 6-3. Again, the predictions of temperature at the steam generator inlet from the nonlinear version of the RO-TPD-PWR simulator most closely match those of the full-scope TPD-GPWR simulator. Although the discrepancies in the predictions of the feedwater temperature appear larger than the discrepancies shown in Figures 6-2 and 6-3, the impact of the differences is not as large as first glance might indicate. The difference in enthalpy of the condensate in the feedwater heaters compared to the enthalpy of the steam in the main steam line is actually the mechanism that drives the decrease in main steam flow with increasing thermal power dispatch. Due to the large enthalpy difference between liquid water and water vapor, the percent differences between the

predicted enthalpies of the condensate entering the steam generator is less than 11% compared to the enthalpy of the steam exiting the steam generator.

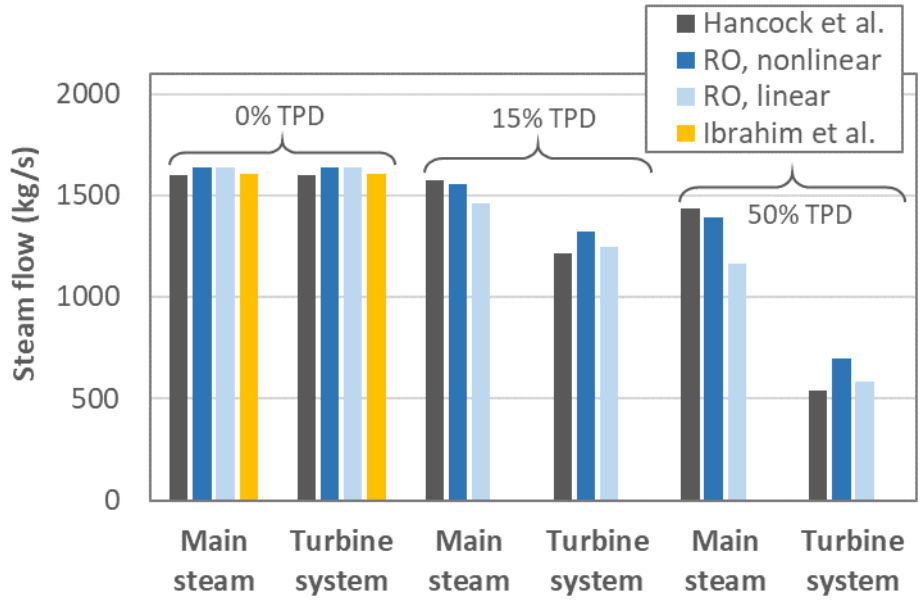

Figure 6-2. Predicted steam flow in the main steam line and turbine system for 0%, 15% and 50% TPD according to a full-scope TPD-GPWR simulator (Hancock et al), an approximate PWR mathematical model proposed by Ibrahim et al (0% TPD only) [5], and two versions of the RO-TPD-PWR simulator.

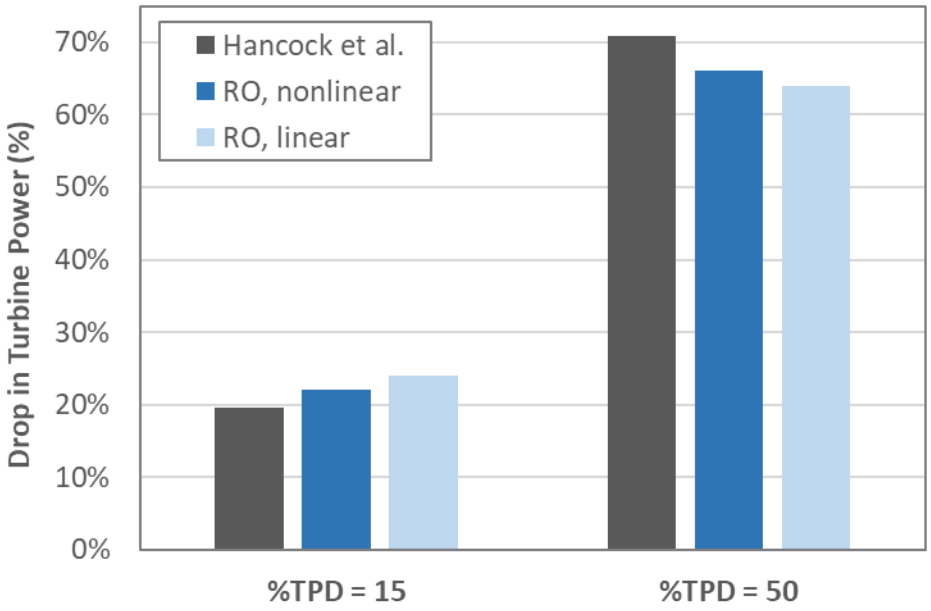

Figure 6-3. Predicted drop in turbine power output for 15% and 50% TPD according to a full-scope TPD-GPWR simulator (Hancock et al) and two versions of the RO-TPD-PWR simulator.

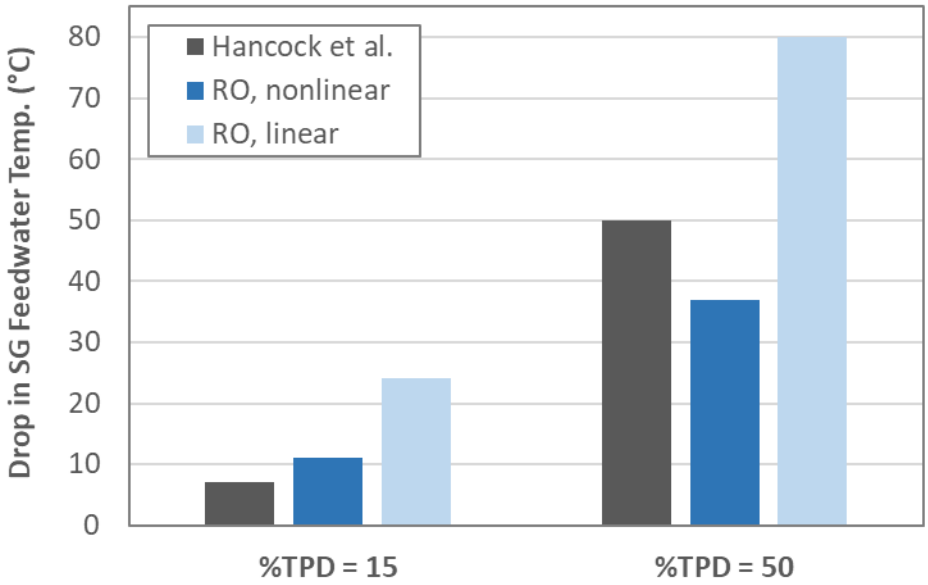

Figure 6-4. Predicted drop in steam generator feedwater inlet temperature for 15% and 50% TPD according to a full-scope TPD-GPWR simulator (Hancock et al) and two versions of the RO-TPD-PWR simulator.

Based on the results presented above, it is determined that predictions of key parameter values by the RO-TPD-PWR simulator match those of the full-scope TPD-GPWR simulator within +/-15%, which meets the goal described in Section 1 (greater than 85% agreement for key parameters, such as the mass flow rates and fluid enthalpies in the main steam line, turbine system, and the thermal power dispatch system). This same model formulation has been shown to be capable of predicting the performance of a 60 MW SMR with similar accuracy [2], indicating it is capable of scaling to different plant sizes. The ability to scale between lab-size equipment (~100 kW) and full-scale nuclear power plants (~1 GW) by adjusting only a few parameters in the models, such as fluid masses and heat exchanger areas (as listed in Appendix B) is a key purpose of the RO-TPD-PWR. The ability of the model to match experimental measurements using pilot-scale equipment at INL will be established when that data becomes available. The Thermal Energy Distribution System (TEDS) is currently being commissioned and operational data is expected by September 2021. INL is also working with Bloom Energy to install a 100 kW high temperature electrolysis (HTE) unit at INL in August of 2021, and data from that system is also expected to also be available by September 2021 to demonstrate the ability of the RO-TPD-PWR simulator to match measurements of relevant pilot-scale equipment.

A final point is that the relative simplicity of the RO-TPD-PWR simulator has proven highly valuable in interpreting and explaining results obtained from the full-scope TPD-GPWR simulator. The RO-TPD-PWR simulator has proven beneficial in explaining nuanced key relationships between parameters, includes those between steam flows in the TPD system, turbine system, feedwater heaters and the main steam lines.

7. CONCLUSIONS AND RECOMMENDATIONS

This report describes the development, modeling, and results of a reduced-order thermal power dispatch pressurized water reactor (RO-TPD-PWR) power plant simulator that incorporates coupled electrical and thermal power dispatch to an industrial process. The simulator is built on models that have been developed in previous work, including a Rancor Microworld model previously developed by INL

and the University of Idaho [1] and reactor core and secondary system models that have been published previously [2].

Results presented in this work show that predictions of key parameter values by the RO-TPD-PWR simulator match those of the full-scope TPD-GPWR simulator within +/-15%, which meets the goal of the project (greater than 85% agreement for key parameters, such as the mass flow rates and fluid enthalpies in the main steam line, turbine system, and the thermal power dispatch system). Simulation results have been presented for two levels of thermal power dispatch, including 15% and 50% of the full reactor thermal power. Thermal power dispatch levels of 15% and 50% were chosen because they are approximately the amounts needed for high efficiency production of hydrogen and synthetic fuels, respectively. Those values also match simulations that have been performed using a full-scope TPD-GPWR simulator [4]. The design and approach used for the RO-TPD-GPWR simulator have also matched those of the full-scope-GPWR simulator to facilitate comparison of results. In this effort, the relative simplicity of the RO-TPD-PWR simulator has proven highly valuable in interpreting and explaining results obtained from the full-scope TPD-GPWR simulator. The RO-TPD-PWR simulator has proven beneficial in explaining nuanced key relationships between parameters, includes those between steam flows in the TPD system, turbine system, feedwater heaters and the main steam lines.

The ability to scale between lab-size equipment (~100 kW) and full-scale nuclear power plants (~1 GW) by adjusting only a few parameters in the models, such as fluid masses and heat exchanger areas (as listed in Appendix B) is a key purpose of the RO-TPD-PWR. The ability of the model to match experimental measurements using pilot-scale equipment at INL will be established when that data becomes available. The Thermal Energy Distribution System (TEDS) is currently being commissioned at INL and operational data is expected by September 2021. INL is also working with Bloom Energy to install a 100 kW high temperature electrolysis (HTE) unit at INL in August of 2021, and data from that system is also expected to also be available by September 2021 to demonstrate the ability of the RO-TPD-PWR simulator to match measurements of relevant pilot-scale equipment.

Coupling of electric power is based on connecting the simulator to real-time digital power simulation (DRTS) capabilities at INL. A feasibility study of electrical coupling was performed and summarized in Section 2. Simulated industrial loads less than approximately 60 MWe can be couped to the TPD-GPWR as a house load while still being able to meet the requirement that a single unit auxiliary transformer (UAT) be able to support all auxiliary loads. The electrical connection to industrial loads larger than 60 MWe will need to follow a standard industrial facility connection to the bulk power grid in which the power connection is made on the high voltage side of the Generator Step-Up (GSU) transformer to protect the main generator of the NPP from sudden trips at the hydrogen plant or failures of the transmission line.

The baseline operation of the TPD-GPWR simulator comes with three principal operating TPD modes of the integrated nuclear power/hydrogen production system which are:

A. Cold Shutdown – the extraction steam line (XSL) has zero flow and is at ambient temperature;

B. Hot Standby – the XSL has minimal flow to maintain hot conditions in both lines and at the hydrogen plant;

C. Thermal power dispatch (TPD) – the XSL has sufficient flow to provide the desired thermal power to the industrial process.

The transition from Hot Standby to TPD is an important task for this effort because it may be a frequently used procedure and it may involve substantial and rapid changes in thermal power flow while also maintaining the NPP reactor at near full thermal power generation. Simulation results show that this transition can be readily accomplished.

All versions of the RO-TPD-PWR and full-scope TPD-GPWR simulators developed so far have sought to keep the design as simple as reasonably possible by extracting steam from the main steam line, removing as much heat as practical from that steam and then returning the condensate to the condenser. The design of the TPD system can be optimized to reduce the impact on the NPP operations, especially the turbine generator system, the condenser, and the feed water heater trains. Steam of sufficient temperature and quality for high temperature electrolysis (HTE) can be extracted from the turbine system. For example, the temperature of steam at the hydrogen plant only needs to be approximately 120 °C, and steam between 200 and 240 °C can be extracted from the high pressure (HP) turbine. Also, condensate from the extraction steam line (XSL) is hotter than condensate in the NPP condenser and could be returned to the feed water heater train to avoid the waste of enthalpy and support heating the feed water. A simplified diagram of this improved TPD system is shown in Figure 7-1. These improvements will be explored in future versions of both the full-scope and reduced-order TPD-PWR simulators.

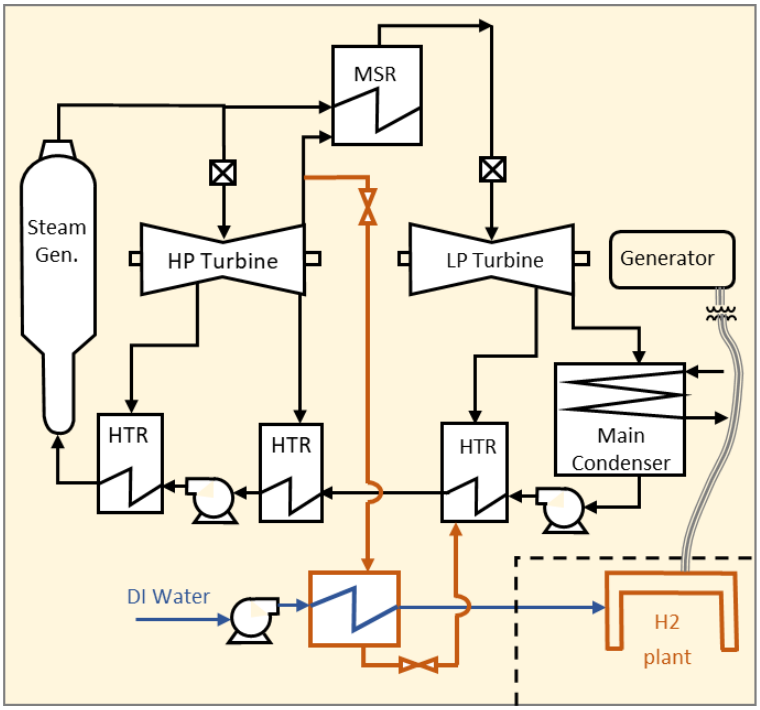

Figure 7-1. Simplified diagram of the PWR modified to dispatch thermal power to a high temperature electrolysis (HTE) hydrogen production plant.

8. REFERENCES

[1] Ulrich T., Boring R., Lew R. (2019) Extrapolating Nuclear Process Control Microworld Simulation Performance Data from Novices to Experts - A Preliminary Analysis. In: Boring R. (eds) Advances in Human Error, Reliability, Resilience, and Performance. AHFE 2018. Advances in Intelligent Systems and Computing, vol 778. Springer, Cham. https://doi.org/10.1007/978-3-319-94391-6_26. Accessed 07-30-2021.

[2] Poudel B., Joshi K., Gokaraju R. (2020) A Dynamic Model of Small Modular Reactor Based Nuclear Plant for Power System Studies. IEEE Trans. Energy Conversion, vol. 35(2), pp 977-985. doi: 10.1109/TEC.2019.2956707.

[3] Westover TL., Hancock S. A. (2020) Shigrekar. Monitoring and Control Systems Technical Guidance for LWR Thermal Energy Delivery. INL/EXT-20-57577.

[4] Hancock S., Westover TL., Luo Y. (2021) Evaluation of Different Levels of Electric and Thermal Power Dispatch Using a Full-Scope PWR Simulator. INL/LTD-21-63226.

[5] Ibrahim SMA., Ibrahim MMA., Attia SI. (2014) The Impact of Climate Changes on the Thermal Performance of a Proposed Pressurized Water Reactor: Nuclear-Power Plant, Internat. J. of Nucl. Energy, vol. 2014, Article ID 793908. https://doi.org/10.1155/2014/793908.

[6] Kerlin TW., Katz E., Thakkar JG., J. E. Strange JE. (1976) Theoretical and experimental dynamic analysis of the H. B. robinson nuclear plant, Nucl. Technol., vol. 30(3), pp. 299–316, 1976.

[7] Ali MRA. (1976) Lumped parameter, state variable dynamic models for Utube recirculation type nuclear steam generators," Ph.D. dissertation, Dept. Nucl. Eng., University of Tennessee, Knoxville, TN, USA.

APPENDIX A: Additional Thermal Power Dispatch Figures

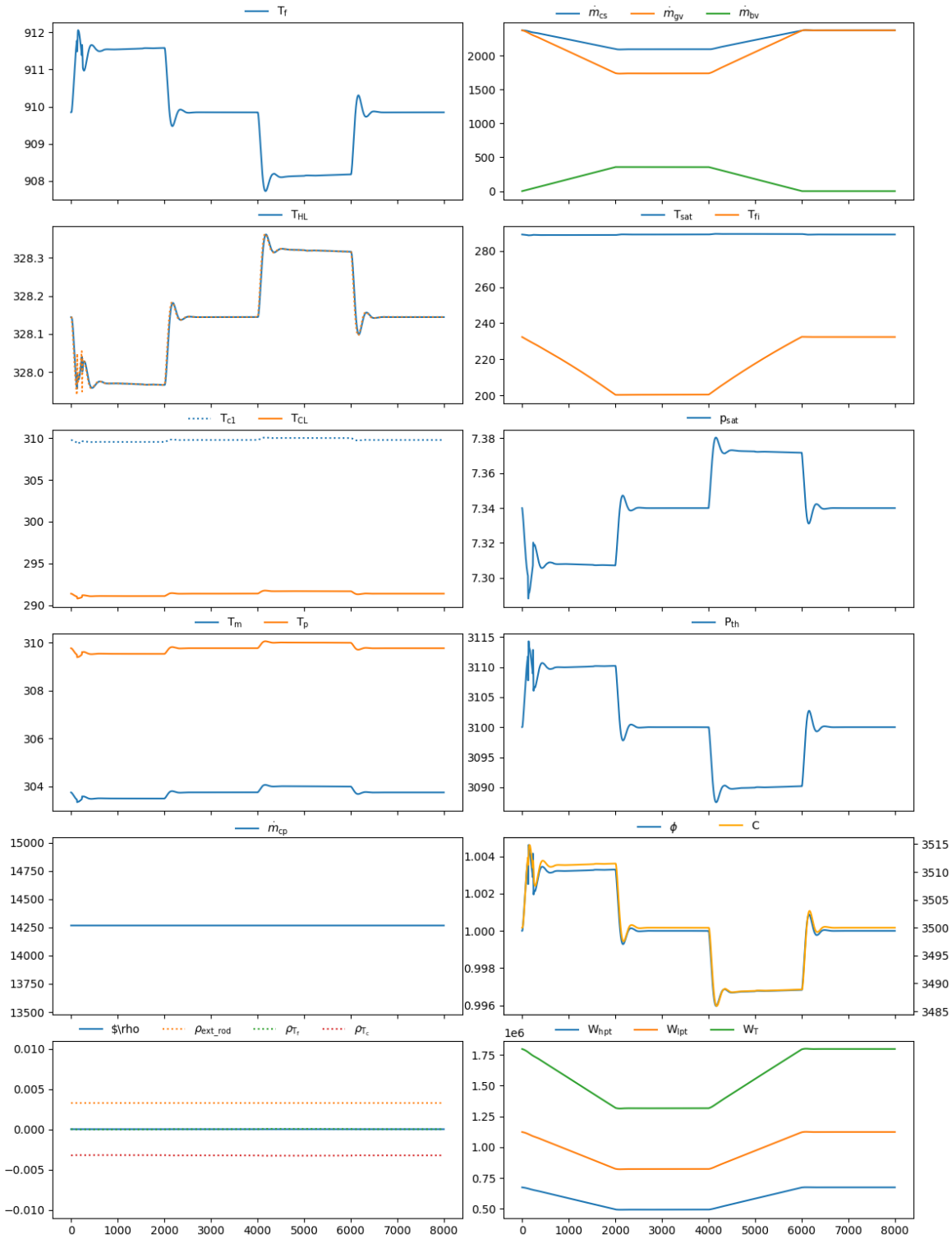

Figure A-1. Predicted timeseries of key parameters for 15% TPD. Definitions of symbols are below.

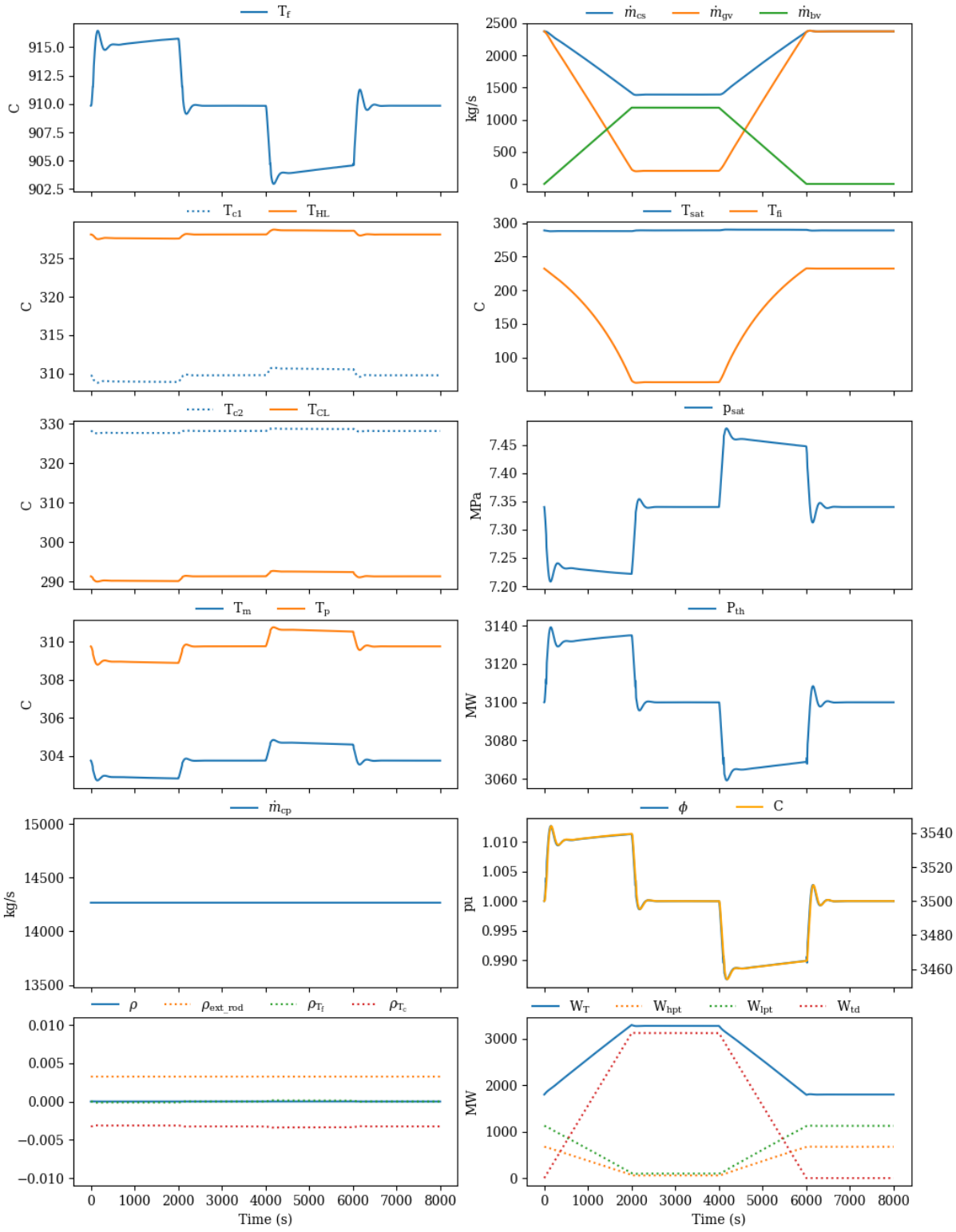

Figure A-2. Predicted timeseries of key parameters for 50% TPD. Definitions of symbols are below.

Definitions of symbols used in Figures B-1 and B-2 are:

- T_f - Temperature of the fuel (C)
- T_c1, T_c2 - Temperature of nodes in the reactor
- T_HL - T of Hot leg
- T_CL - T of Cold leg
- T_m - T of the SG metal lump
- T_p - T of the primary coolant in the SG
- m_cp - primary coolant flow (kg/s)
- rho - total reactor rhow
- rho_ext_rod - external rhow
- rho_tau_f - fuel temperature feedback
- rho_tau_c - coolant temperature feedback
- m_cs - secondary steam flow
- m_gv - steam flow to turbine
- m_bv - steam to thermal delivery loop
- T_sat - saturation temperature of secondary in the SG
- T_fi - feedwater temperature to SG
- p_sat - saturation pressure in SG (MPa)
- P_th - thermal power (MW)
- phi - average neutron flux
- C - neutronics model count
- W_T - total power (kJ/s)
- W_hpt - HPT power calculated from flow and enthalpy drop
- W_lpt - LPT power calculated form flow and enthalpy drop

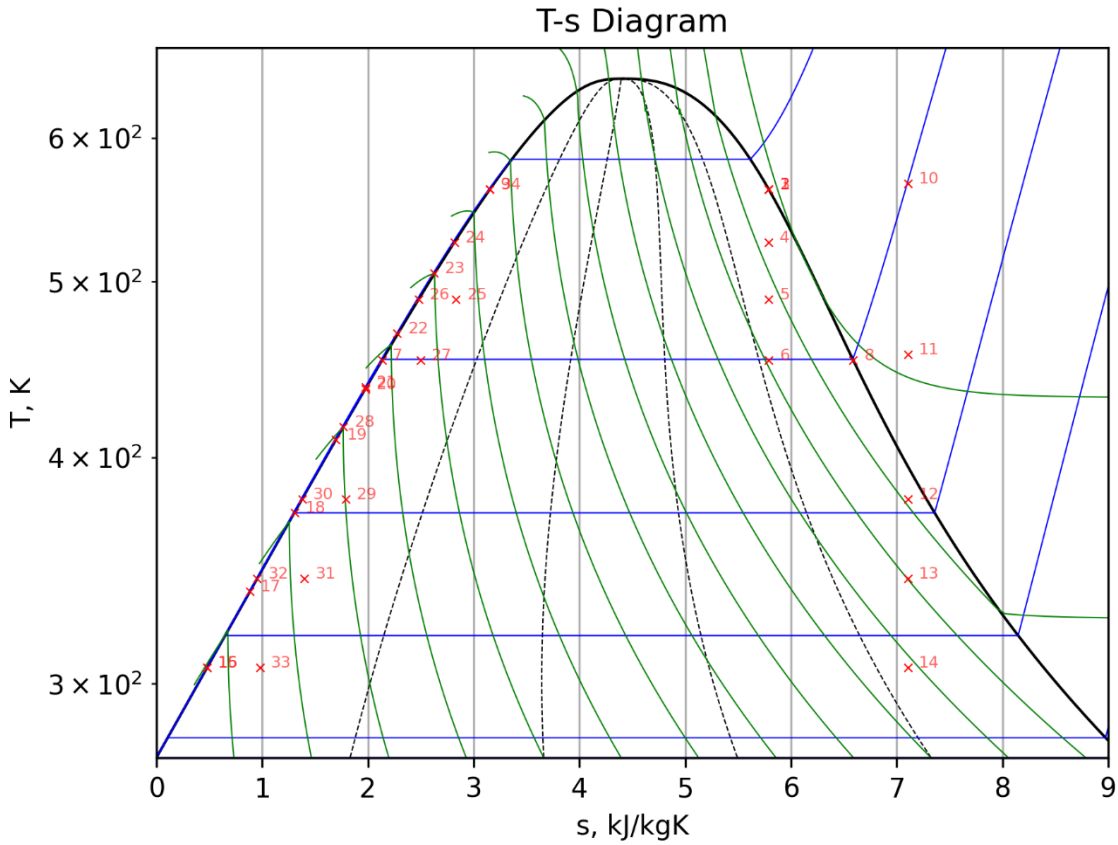

Figure A-3. T-S diagram for the secondary system in the RO-TPD-PWR simulation for 0% TDP.

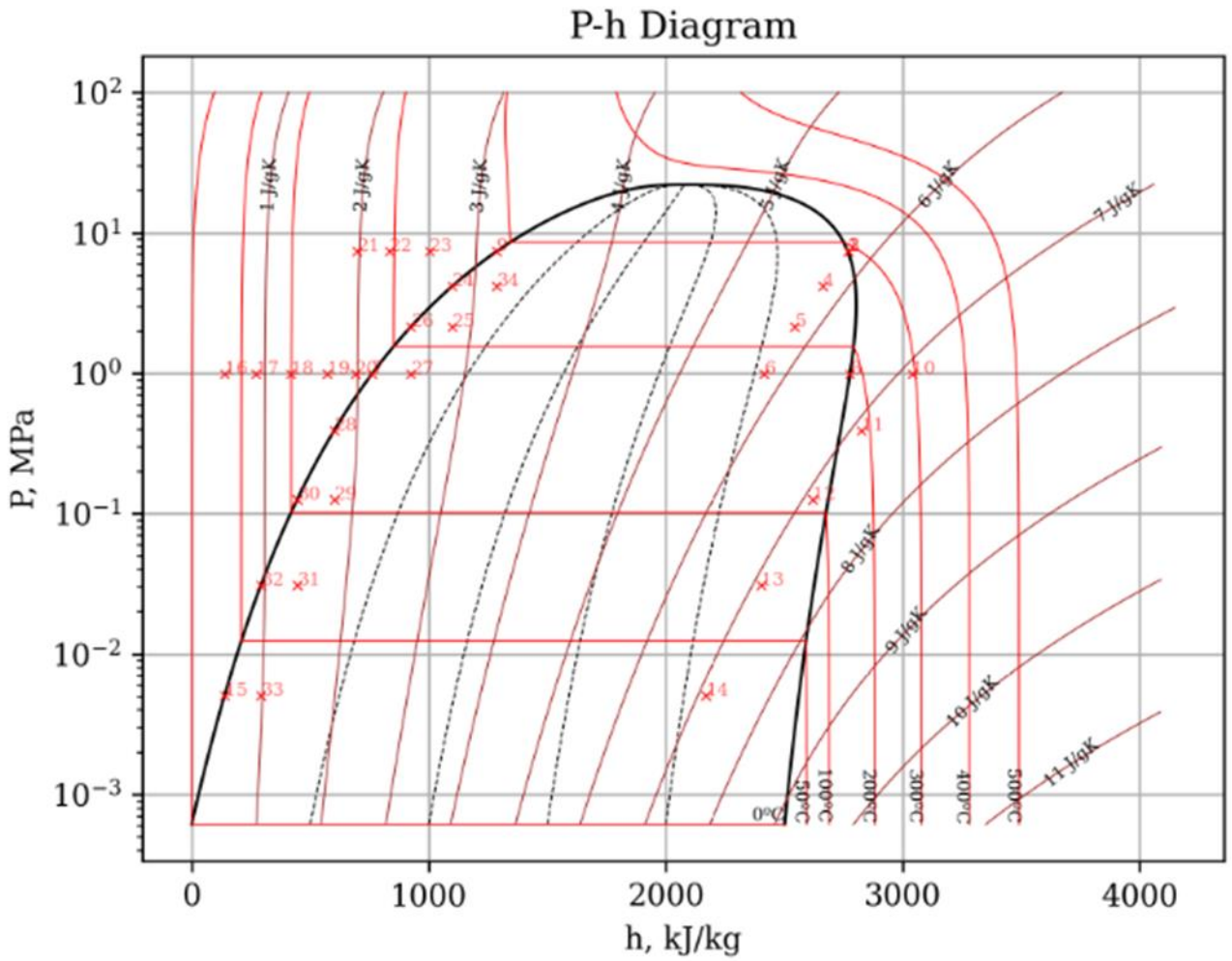

Figure A-4. P-h diagram for the secondary system in the RO-TPD-PWR simulation for 0% TDP.

APPENDIX B: Initial Values of Parameters

Parameter	Class	Description	Units	SMR	GPWR
time_step	Simulation	step for simulation	s	0.01	0.01
alpha_f	Neutronics	fuel temperature feedback coefficient	reactivity/degc	-0.0000216	-0.0000216
alpha_c	Neutronics	moderator temperature feedback coefficient	reactivity/degc	-0.00018	-0.00018
Beta	Neutronics	delayed neutron fraction		0.007	0.007
Lambda	Neutronics	prompt neutron life	s	0.00002	0.00002
_lambda	Neutronics	decay constant	1/s	0.1	0.1
phi	Neutronics	Average Neutron Flux	pu	1	1
rho	Neutronics	Net core reactivity		0	0
C	Neutronics			2800	2800
T_f_0	Reactor	initial fuel temperature	C	488.09	613.51
T_f	Reactor	fuel temperature	C	T_f_0	T_f_0
tau	Reactor	fraction of thermal power in the fuel	fraction	0.67	0.67
P_100	Reactor	thermal rated power	MW	160	2900
P_th_0	Reactor	initial instantaneous power	MW	P_100	P_100
P_th	Reactor	instantaneous power	MW	P_th_0	P_th_0
m_f	Fuel	mass of the fuel lump	kg	11252	86290.30234
v_f	Fuel	volume of the fuel lump	m^3	1.025706472	7.866025738
h_fc	Fuel	heat transfer coefficient of fuel to coolant	W/(m^2 * C)	1135	1135
A_fc	Fuel	effective heat transfer of fuel to coolant	m^2	583	4415.462917
c_pf	Fuel	specific heat capacity of fuel lump	kJ / (kg * C)	0.467	0.467
v_c	Primary	volume of the primary reactor vessel	m^3	1.879	159.8895786
mdot_cp_100	Primary	mass flow rate of the primary coolant at rated power	kg/s	586.86	14267.58
mdot_cp	Primary	mass flow rate of the primary coolant	kg/s	mdot_cp_100 * (P_th / P_100) ** (1.0 / 3.0)	mdot_cp_100

T_CL_0	ColdLoop	initial cold loop temperature	C	219.92	291.66
T_CL	ColdLoop	cold loop temperature	C	T_CL_0	T_CL_0
v_CL	ColdLoop	cold loop volume	m^3	26.8	14.18
T_c2_0	Reactor	initial c2 node temperature	C	T_CL	T_CL
T_c2	Reactor	initial c2 node temperature	C	T_c2_0	T_c2_0
T_HL_0	ColdLoop	initial cold loop temperature	C	255	326
T_HL	ColdLoop	cold loop temperature	C	T_CL_0	T_CL_0
v_HL	ColdLoop	cold loop volume	m^3	9.7	14
T_c1_0	Reactor	initial c2 node temperature	C	T_HL	T_HL
T_c1	Reactor	initial c2 node temperature	C	T_c1_0	T_c1_0
T_p_0	Steam Generator	initial average temperature of the primary coolant in the sg region	C	240	309.4444444
T_p	Steam Generator	average temperature of the primary coolant in the sg region	C	T_p_0	T_p_0
T_p_ref	SteamGenerator	reference temperature for rod control	C	T_p_0	T_p_0
v_p	SteamGenerator	volume of the primary coolant region in the sg	m^3	3.564	0
h_pm	SteamGenerator	heat transfer coefficient of primary to metal lump	W/(m^2 * C)	20391	20391
A_pm	SteamGenerator	heat transfer area of primary to metal lump	m^2	1123	4143.276847
T_m_0	SteamGenerator	initial temperature of the sg metal lump	C	249	300
T_m	SteamGenerator	temperature of the sg metal lump	C	T_m_0	T_m_0
m_m	SteamGenerator	mass of the sg metal lump	kg	7869	62019.49091

c_m	SteamGenerator	specific heat capacity of sg metal lump	kJ / (kg * C)	0.45	0.45
h_ms	SteamGenerator	heat transfer coefficient sg metal lump to secondary	W/(m^2 * C)	4950	4950
A_ms	SteamGenerator	heat transfer area of sg metal lump to secondary	m^2	1214	6986.308608
T_sat	SteamGenerator	saturation temperature in the sg region	C	f(p_sat)	f(p_sat)
sg_level	SteamGenerator	fraction of water in the sg by volume	fraction	0.322679412	
p_sat_0	SteamGenerator	initial secondary steam pressure	MPa	2.71	6.89
p_sat	SteamGenerator	secondary steam pressure	MPa	p_sat_0	p_sat_0
mdot_cs_0	FeedWater	initial secondary feedwater flow	kg/s	77.93	1620
mdot_cs	FeedWater	secondary feedwater flow	kg/s	mdot_cs_0	mdot_cs_0
mdot_cv	MainSteam	secondary main steam flow	kg/s	mdot_cs_0	mdot_cs_0
T_fi_0	FeedWater	initial feedwater temperature	C	170	223
T_fi	FeedWater	feedwater temperature	C	T_fi_0	T_fi_0
v_sg	SteamGenerator	sg secondary side volume	m^3	13.391	70.08
rod_control_Kp	RodControl	rod control proportional gain		0.0005	0.0005
rod_control_Ki	RodControl	rod control integrative gain		0.00005	0.00005